PULSED LASER HETEROEPITAXY OF HIGH QUALITY CDTE THIN FILMS ON SAPPHIRE SUBSTRATES

Pulsed Laser Heteroepitaxy of High Quality CdTe Thin Films on Sapphire Substrates

By

Stephen Michael Jovanovic, B.Eng.,

A Thesis

Submitted to the School of Graduate Studies

in Partial Fulfilment of the Requirements for the Degree

Master of Applied Science

McMaster University

Master of Applied Science (2013) McMaster University

(Department of Engineering Physics) Hamilton, Ontario

TITLE: Pulsed Laser Heteroepitaxy of High Quality CdTe Thin Films on Sapphire Substrates

AUTHOR: Stephen Michael Jovanovic, B.Eng., (McMaster University)

SUPERVISOR: Dr. John S. Preston

Abstract

The growth of CdTe thin films on Al_2O_3 (0001) substrates by pulsed laser deposition from undoped pressed powder targets was studied. Thin film crystal structure was investigated by x-ray texture analysis as a function of plume flux, growth temperature and film thickness. Crystal texture increased for a decrease in plume flux. Single crystal CdTe (111) films were obtained by optimizing the plume flux. Increasing the growth temperature demonstrated a reduction in twin density. An optimum temperature of 300°C minimized the twin density without adverse desorption effects. The twin density decreased as an inverse squared function of film thickness. Single crystal CdTe films with comparable structural quality to Bridgeman single crystal wafers were grown under optimal conditions.

The optoelectronic properties of CdTe films were investigated by photoluminescence and photoreflectance spectroscopy. The room temperature bandgap energy of 1.51 eV was consistent between spectroscopic measurements. Broadening parameters for spectra were consistent with reference high quality material. Low temperature photoluminescence spectra had a dominant emission consistent with bound excitons found in bulk CdTe. Emissions consistent with self-compensation or doping were not found. Hall effect and conductivity measurements at 300 K demonstrated high resistivity for undoped material and electron mobilities comparable to bulk CdTe for lightly doped films. Spectroscopic

and electrical measurements of high structural quality CdTe films were consistent with high optoelectronic quality.

An as-grown ability of the films to detach from their substrate was discovered. X-ray texture analysis and photoluminescence spectroscopy of films released onto rigid secondary carriers demonstrated that they maintained their structural and optoelectronic quality proceeding lift-off. Substrates having films released from them were found to be suitable for repeated growth. The technological relevance of this discovery is likely to drive further study into the lift-off phenomena and controlled doping of CdTe thin films.

Acknowledgments

I would like to gratefully acknowledge and thank the following for their help and support during the course of my Master's studies at McMaster:

The National Sciences and Engineering Research Council of Canada Collaborative Research and Training Experience Program in Photovoltaics for funding and support of this project.

My supervisor, Professor John Stuart Preston, for giving me the opportunity to work on this project as well as steadfast mentorship, guidance, and motivation.

Doris V. Stevanovic, Dr. James F. Britten, Jim Garrett, Peter Jonasson and Zhilin Peng who provided me with training and support on facility equipment.

My colleagues Dr. Christopher Haapamaki, Gabriel A. Devenyi, Dr. Jessica Carvalho, Dr. Kristoffer Meinander, Paul Kuyanov and Victoria Jarvis for prolific discussion, ideas, advice and experimental collaboration.

My parents, John and Kathy, grandparents, Lois, Nerina, Paul and Svetomir, brothers, Andrew and Paul, for their resolute belief in me, support, and sacrifices on my behalf.

My better half, Tahereh Majdi, who as a source of inspiration, confidence, and unwavering support helped me get to where I am today.

Stephen M. Jovanovic

Listing of Contents

Listing of Figures

Listing of Tables

Chapter 1 - Introduction

The development of the first transistor in 1947 marked the beginning of a new materials age. With it came the need, and subsequent ability, to produce defect free single crystals with purity levels as high as 99.999% (5N). Cadmium telluride (CdTe) is perhaps the most important II-VI semiconducting compound. It typifies the difficulties surrounding both semiconductor materials research and processing in this category of semiconductors. Unlike elemental and group III-V semiconductors such as silicon, germanium, gallium arsenide and indium antimonide, high quality CdTe materials have developed slowly.

This slow development pace is peculiar because of the industrial relevance of CdTe and can be attributed to both a lack of structural material knowledge and processing difficulties. In particular, a series of point defects and complexes exist uniquely for II-VI semiconductors because of their ionic bonding, whereas IV and III-V semiconductors have covalent bonding. Further contrasting IV and III-V semiconductors, II-VI semiconductors easily form dislocations, stacking faults and inclusions which create substantial processing difficulties. Therefore, while current CdTe device technologies can be improved within their parameter space by experimental optimization, it is only with detailed materials knowledge that they can be mastered.

1.1 Crystal Structure

Like other II-VI semiconductors CdTe can crystallize in both a cubic, zinc blende (ZB), and hexagonal, wurtzite (WZ), structures with lattice constants of a_z=6.481 Å [1] and a_w=4.58 Å/c_w=7.50 Å [2] respectively, as seen in Figure 1. While bulk CdTe crystals are of the cubic form thin films may also be of the hexagonal form. The energy of formation difference between these two structures is small, as low as 9 meV/2 atoms [3], leading to correspondingly low stacking fault energies.

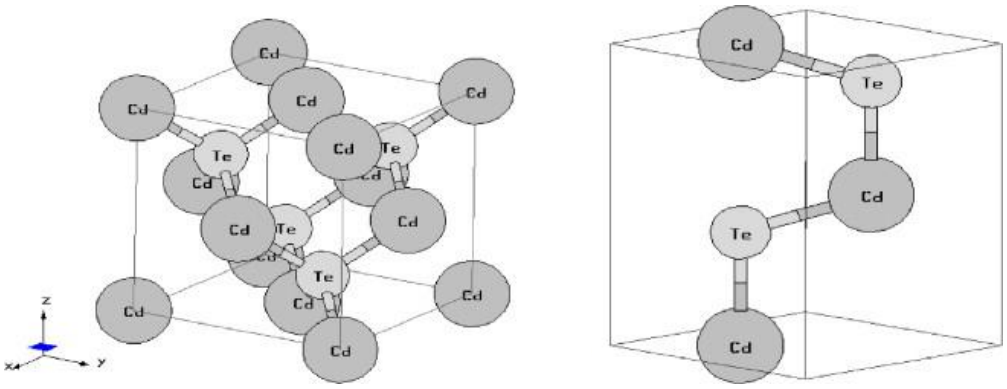

Figure 1: CdTe (Left) ZB and (Right) WZ Unit Cells, Modified from [4]

The ZB structure can be interpreted as two interpenetrating face centered cubic sublattices translated by $\frac{1}{4}$ of the body diagonal. This gives a nearest neighbour distance of $\frac{\sqrt{3}a}{4}$. CdTe films have a well-established propensity to form their (111) plane parallel to the substrate, as such, a more convenient understanding of the CdTe ZB structure is found normal to the (111) plane [5]. The stacking sequence of close packed planes are (111) oriented and arranged tetrahedrally. Alternatively this can be visualized as layers

composed of alternating Cd and Te atoms. Without centro-symmetry the structure has crystallographic polarity where the (111) face is either terminated by Cd or Te, triply bonded to the atoms beneath. Tetrahedral bonding implies that the addition of Cd or Te adatoms to a Te or Cd terminated surface will lead to the formation of a single bond less stable than those below with three bonds. It is therefore expected stabilized surfaces are terminated solely with Cd or Te, designated as A and B terminated respectively. The surfaces are described with orientation and polarity as (111)A or (111)B.

The WZ structure of CdTe is seemingly different than the ZB structure, but is quite similar. Normal to the ZB (111) plane in CdTe, the two dimensional layers are offset relative from each other in three unique positions, giving rise to six-fold symmetry. In the [0001] direction of the WZ CdTe crystal the Cd and Te layers are offset in two unique positions and therefore the stacking sequence repeats in four layers opposed to the required six for the ZB structure. The θ-2θ x-ray diffraction technique used for semiconductor structural characterization, which is sensitive only to periodicities normal to the substrates surface, cannot therefore easily distinguish between the two structures. Due to this, in practise, CdTe films are often structurally mischaracterized. Two-dimensional x-ray diffraction (2DXRD) can be used as an alternative characterization technique to determine the contributions of both ZB and WZ planes in a CdTe crystal [6]. Mixed structure films have been studied and it has been proposed that WZ layers in ZB films may act as hole trap centres [7].

While structural characterization studies extended of defects, electro-optical characterization completes the material picture studying the electrical effects of extended and point defects. Since defects such as dislocations, incoherent twin and grain boundaries, stacking faults and inclusions can lead to degradation of device performance electro-optically their passivation, suppression and mitigation are of importance to improve processability. The creation of high quality single crystalline CdTe is therefore a milestone into the investigation of how extended and point defects shift material and device behaviours from ideal.

1.2 Band Structure

The unique and commercially exploitable optoelectronic properties of CdTe arise from its electronic band structure. The band structure solution can be arrived at empirically or ab-initio by a variety of methods [8], [9], [10]. A starting point in the consideration of the CdTe band structure is a bond orbital approximation for the ZB structure. The relationship between the binding energy and the equilibrium bond length, d_0, is given below in Equation 1 [11]:

$$E_b - \xi \simeq \begin{cases} \frac{-A}{2d_0^2}, & V_2 \gg V_3 \\ -V_3, & V_3 \gg V_2 \end{cases} \qquad \textbf{Equation 1}$$

Where $E_b - \xi$ is the net bond energy, A accounts for the average electron energy per atom, V_2 is the covalent energy and V_3 is the polar energy. The equality states that the bond orbital model predicts that the binding energy of purely covalent materials increases as the inverse square of the bond length, while ionic materials have binding energy

independent of bond length. This trend can be verified experimentally looking at the bond lengths of covalent materials, such as VI and III-V semiconductors, comparatively with ionic materials, such as II-VI semiconductors, in relation to their melting points. II-VI semiconductors often have a higher melting point than VI and III-V semiconductors of equivalent atomic bond length indicating higher binding strength. While pure ionic bonding does not exist, a high percentage of ionic bonding, such as 71% ionic for CdTe [12], is considered to be ionic dominated bonding.

The band structure analysis of CdTe and other II-VI semiconductors is more complicated than for IV and III-V semiconductors, in part due to their ionic nature, due to a strong sp-d orbital interaction [10]. Although the initial important aspects of the CdTe band structure, such as having a direct bandgap, came about from pseudopotential approaches, as seen in Figure 2, it was not until the application of ab-initio methods that strong empirical and theoretical agreement was achieved [13]. Local density approximation estimates of CdTe's bandgap overestimated the contribution of semi-core d-orbital states and as a result underestimated the bandgap, predicting 0.2 eV instead of the empirically determined 1.6 eV at 0 K [11]. These methods were improved by perturbative Green's function screened potential (GW) approximations [13].

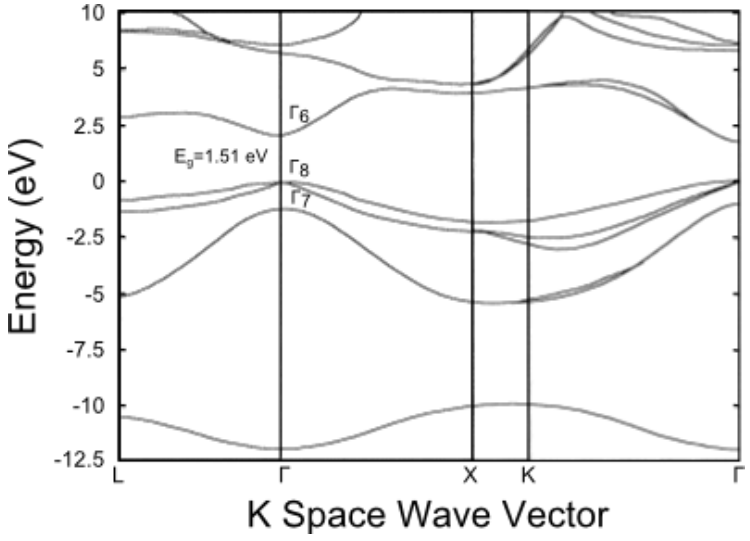

Figure 2: CdTe Band Structure Calculated by Pseudoempirical Methods, Modified from [14]

CdTe has a reported direct bandgap at 300 K of 1.51 eV; depending on the material quality and conductivity literature values for this number can vary [15]. There is some contention in literature about whether CdTe is indirect or direct since its direct and indirect minimum gap energies are close [16]. However, due to the large absorption coefficient of CdTe over the wavelengths of interest and short carrier lifetimes, discussions in this thesis will assume that direct transitions dominate. As indicated by the concavity of the band structure the electron, light hole and heavy hole masses are small which leads to high mobility. The effective electron, light hole and heavily hole masses determined from cyclotron resonances or Faraday rotation are $0.11m_0$ [17], [18], $0.12m_0$ and $0.84m_0$ [19] respectively. The electron effective mass appears independent of carrier concentration up to $1.7x10^{18}$ cm^{-3} [17] and the mentioned hole effective masses are for the [111] direction in CdTe.

As a semiconductor, the electrical and optical behaviour of CdTe can be modified by the extrinsic and intrinsic dopants with energy levels that lie within the forbidden zone. Figure 3 illustrates a variety of intrinsic and extrinsic dopant energy levels, both acceptor and donor, in the CdTe band structure.

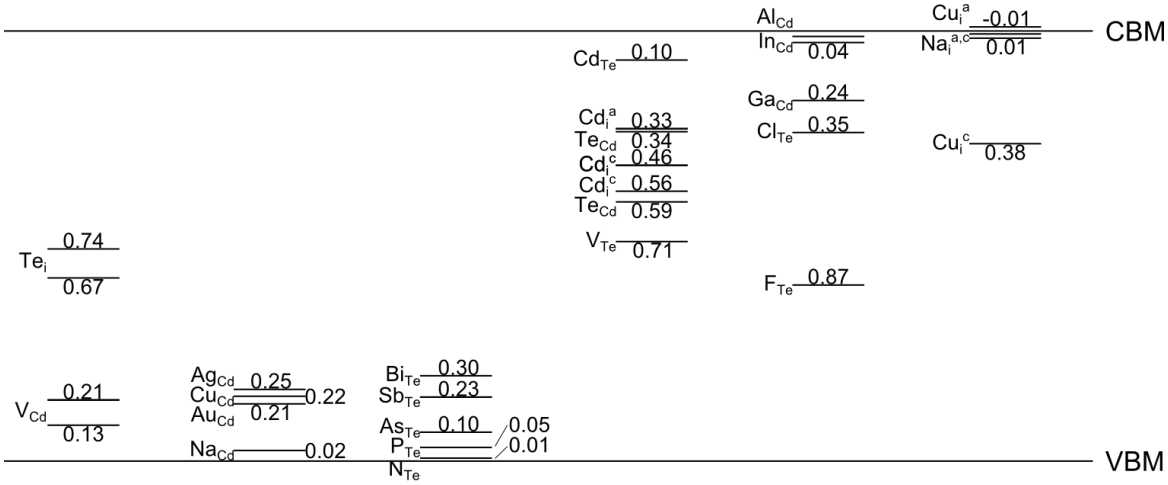

Figure 3: Various Calculated Intrinsic and Extrinsic Acceptor and Donor Transition Energy Levels in CdTe Modified from [20]

Vacancies on a cadmium site, V_{Cd}, and a cadmium substitution on a tellurium site, Cd_{Te}, have transition energy levels in CdTe suitable for p-type and n-type self-compensation of extrinsic dopants. From a neutral charge state the formation energy for V_{Cd} and Cd_{Te} are quite high, 2.67 eV and 3.92 eV respectively. However, empirical analysis of II-VI semiconductor doping show that the introduction of dopants form oppositely charged native point defects through lowering the formation energy of intrinsic dopants in thermodynamic equilibrium. The energy of formation for self-compensating defects is further complicated by associative compensation, the formation of complexes containing both the extrinsic impurity and a native point defect. This phenomenon was

modelled by Mandel and is sometime referred to as Fermi level induced compensation [21]. Fermi level dependent self-compensation is not expected in traditional VI and III-V semiconductors and adds complexity to both the processing and analysis of II-VI semiconductors. A full table of the formation energies for the donors and acceptors seen in Figure 3, from a neutral charge state, can be found in Appendix A.

Self-compensation in II-VI semiconductors is an ongoing materials issue for a variety of CdTe devices. It does, however, have benefits for devices requiring high resistivity such as radiation detectors. Figure 4 is a summary of experimentally achieved maximum carrier concentrations achieved in various II-VI semiconductors.

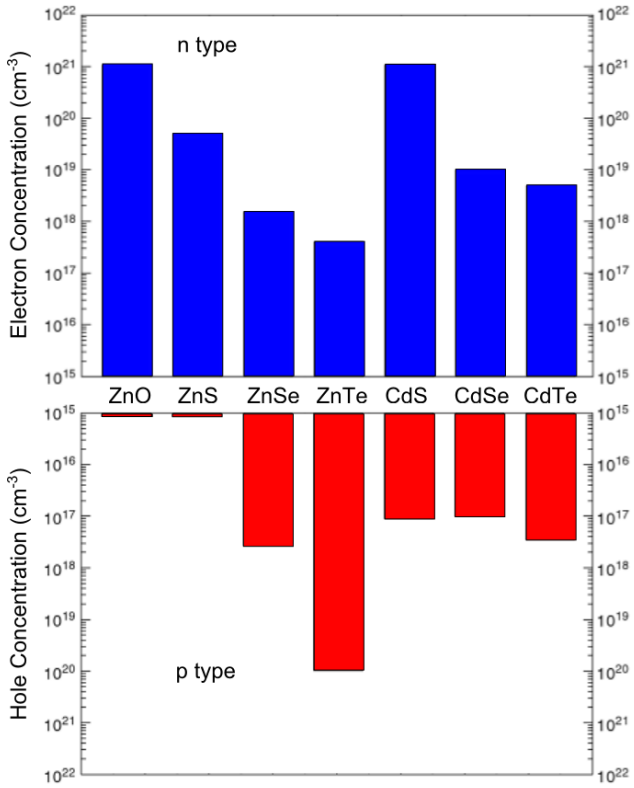

Figure 4: Experimental Maximum Carrier Concentration in Various II-VI Semiconductors, Modified from [11]

The maximum electron and hole concentration at room temperature for single crystalline CdTe is $5.3x10^{18}$ cm^{-3} [22] and $2.8x10^{17}$ cm^{-3} [23] respectively. These carrier concentrations were achieved with iodine and phosphorus respectively in thermodynamic equilibrium. Non-equilibrium doping such as laser doping [24], ion implantation [25] and the doping of non-stoichiometric CdTe [26] have all been proposed as mechanisms to enhance the doping limits. Since the energy of defect formation is a function of the Fermi energy in CdTe under equilibrium the addition of impurities to form ternary alloys of CdTe, those that raise the valance band edge or lower the conduction band edge, may also be considered to improve doping efficiency. Common ternary alloys of CdTe include $Cd_xZn_{1-x}Te$ (CZT), $Hg_{1-x}Cd_xTe$ (MCT) and $Cd_xMn_{1-x}Te$. Whereas ZnTe is a direct bandgap semiconductor and HgTe is a semimetal, in addition to modifying the doping efficiency ternary alloys of CdTe can be used to create devices which span an absorption range of 2.39 eV to 0 eV.

Point defects can affect CdTe material quality and device performance acting as defects such as traps and scattering centres. They can also modify the CdTe band structure to beget new properties such as modified conductivity and absorbance. The analysis of single crystal CdTe in its undoped stoichiometric form provides a baseline for material quality from which controlled introduction of impurities translates material prowess into device capability.

1.3 Applications of CdTe and Related Ternary Compounds

1.3.1 Infrared Detection

Mercury cadmium telluride is the standard material for infrared detectors with applications ranging from military night vision to deep space infrared telescopy. Dual band infrared detectors, suitable for the mid to long wavelength infrared region, are often called 'two-colour' detectors and consist of focal plane arrays mesa etched into films deposited on epitaxial substrates. These mesa pixels are normally n-p-n devices with the p-region consisting of CdTe [27]. CdTe and CZT are common substrate materials for the growth of MCT; however, the growth of CdTe and its ternary alloys upon the widely available and low cost silicon substrate is often sought after because of the possible integration with silicon based readout integrated circuits. This has been met with limited success on the Si (100) substrate because of the large lattice parameter difference, thermal expansion coefficient and valence mismatch in combination with issues with multi-domain growth [28]. High quality CdTe buffers for MCT have been deposited on (211) Si with etch pit densities in the range of 10^6 cm^{-2} [29], however, this is still two orders of magnitude higher than for lattice matched substrates.

Since CdTe is a buffer layer to MCT growth and integrated electrically into the device a reduction in defect densities provides benefits to performance. While such a reduction on lattice mismatched substrates is possible by such schemes as deposition on miscut substrates [30] or cyclic in-situ annealing [31], surface recombination on the mesa structure still requires significant passivation. A planar structure focal plane array offers

significant benefits to the passivation of devices since the junction interface is buried and therefore schemes to exfoliate planar structures grown on lattice matched substrates have been highly investigated by industry [32]. High quality CdTe buffer layers on sapphire, which is relatively inexpensive compared to CZT, offer an alternative route to meet the industrial demands for MCT devices, particularly with the success of exfoliation and wafer bonding techniques employed with silicon-on-insulator devices.

1.3.2 Radiation Detection

CdTe is one of the most dense and heaviest atomically constituted commercialized semiconductors and consequently has large x-ray and γ-ray radiation absorption cross sections. Furthermore, the isotope ^{113}Cd, with a natural abundance of 12.22%, has a thermal neutron absorption cross section of 20600 barns [33] and is also used for thermal neutron detection. ^{113}Cd acts as a neutron converter, emitting a γ-ray to become ^{114}Cd. As such, neutron detection occurs in the standard detector diode geometry. Given its large bandgap, intrinsic CdTe has a low intrinsic carrier concentration and hence is highly resistive. The resulting low dark current implies minimal thermal noise for radiation detectors. Since detector efficiency for biased devices is related to the number of collected electron-hole pairs per absorbed photon, having a strong bias, low trap density and good transport is beneficial [34].

For applications like medical imaging, security monitoring, nuclear safeguarding and astrophysics a device that operates without the need for cryogenic cooling is preferred [35], [36]. Without the need to cool detectors, digital imaging technology can provide

both superior quality and processing capabilities. Due to CdTe's intrinsic ability to generate point defects and complexes under thermodynamic equilibrium often it is a required to add deep level traps, such as Ge, Sn and Pb or grow under Cd-rich conditions to improve the resistivity for detector applications [37]. As well, since large area arrays are difficult to develop from single crystal boules, high quality thick film technologies on commercially viable substrates are necessary to decrease costs. The growth of undoped single crystal CdTe films provides the basis of high mobility uncompensated material for use in radiation detectors, from which more efficient structures can be created.

1.3.3 Photovoltaics

Certainly CdTe is best known for its application to photovoltaic devices. CdTe photovoltaic devices are often configured in a superstrate configuration in which the glass they are grown on is also the illuminated side. Pointed towards the sun it appears the glass is on top of the active device, unlike substrates which are often under the active device in which they are incorporated. Polycrystalline CdTe solar cells are often grown as a heterostructure with CdS, ZnO or ZnS to improve device open circuit voltage. Current state of the art devices have laboratory efficiencies as high as 17.3% [38] and module efficiencies as high as 14.4% [39]. While predominately used for grid tied home and commercial power generation, because of their light weight and potential for high efficiency, approximately 30% under one sun illumination [40], CdTe solar cells also have application for remote power and satellite application. Silicon wafer based solar cells are the current dominant photovoltaic technology, however, may be displaced by cheaper thin film technologies, such as exfoliated GaAs single junction cells. Thin film

photovoltaic technologies, such as CdTe, have the ability to provide a cost advantage in the required amount of active material, hence, an inexpensive substrate is critical to its commercial success.

Just as silicon-on-insulator technology has adopted exfoliation techniques to achieve thin silicon films, direct gap photovoltaic materials such as GaAs and CdTe grown on lattice matched substrates may also be exfoliated to produce thin film devices of high crystal quality. Since photovoltaics are thermodynamic machines, optical enhancement may also be used to improve performance. Reducing the solid angle of emission from a flat device to the solid angle of the solar source reduces the photon entropy and accordingly increases the maximum recoverable energy in the thermodynamic system. The maximum theoretical efficiency of a single junction cell, optically enhanced, is 40.7%, the same efficiency of a single junction cell under full concentration. Essentially, optical enhancement provides the same reduction in entropy and boost in open circuit voltage as solar concentration provides. This technique has been demonstrated for GaAs exfoliated cells by Alta-Devices [41]. Furthermore, optical enhancement is suited well to thin film direct gap photovoltaics since a decrease in cell thickness for the same absorbed volume increases the device open circuit voltage by reducing the bulk recombination volume as seen in Equation 2. This can alternatively be viewed as their reduced entropy when light-generated minority carriers are produced in a smaller volume, increasing the amount of work that can be done per photon [42].

$$\frac{\partial V_{oc}}{\partial z} = -\frac{kT}{q}\frac{1}{z} \qquad \textbf{Equation 2}$$

Where V_{oc} is the cell open circuit voltage, z is the cell thickness, k is the Boltzmann constant, q is the elementary charge, and T is temperature. This equation is under the assumptions of negligible surface recombination and that the diffusion length is greater than the device thickness.

The properties of CdTe high quality crystals on lattice matched substrates have been considered as a viable alternative to Silicon based technologies. As well, the atoms of CdTe are large and less prone to radiation damage for space applications relative to GaAs. The major issue limiting CdTe photovoltaic technology has been its deposition on inexpensive amorphous substrates like glass which gives rises to associated recombination centers and pinholes. The result is less than optimum open circuit voltages of CdTe, indicative of material quality, for solar cells compared to the nearly maximized short circuit current of similar devices [43]. Beginning with an ideal CdTe crystalline film, devices can be designed in the upper technological limit, similar to research grade GaAs devices, and implemented commercially by the cost reduction of production techniques.

1.4 Review of Previous Relevant Work

Prior 2010, the deposition of CdTe:Ge was explored on a variety of substrates such as MgO (111), $SrTiO_3$ (100), Al_2O_3 (0001) and SiO_2 native oxides on Si (100) using pulsed laser deposition (PLD). Using texture analysis, a 2DXRD analysis technique, it was determined that epitaxial CdTe doped with Germanium (CdTe:Ge) films grew preferentially with their [111] direction perpendicular to the substrate surface. Further, it

was found that single domain CdTe:Ge could be grown on the c-plane of sapphire, where the deposition of a monolayer of Aluminum prior film growth could rotate the domain orientation of CdTe:Ge films by 180°. The main material source target, along with other crystalline CdTe compensated targets, were Bridgman grown single crystal CdTe boules originally studied for vacancy and vacancy complexes using positron annihilation spectroscopy. Since bulk detector grade material is compensated to be resistive, further study of the optoelectronic properties of pure CdTe needed to be conducted on undoped CdTe. Most easily obtained as a pure pressed powder, used in the sputtering of polycrystalline thin films, the PLD recipes of compensated single crystal CdTe targets became the starting point for process optimization on the new class of targets.

1.4.1 The Role of Lattice Mismatch

The growth of CdTe:Ge via PLD on a variety of substrates offering different lattice mismatches revealed a variety of growth characteristics for these films [5]. The substrates chosen were all oxide crystals since the vacuum chamber in which the PLD took place operates only in the high vacuum region, $6x10^{-7}$ Torr. The impingement rate of oxygen in the system is too high to grow on substrates like Si (100) and Si (211).

As previously mentioned films grew preferentially with their (111) planes parallel to the substrates. Preferential [111] alignment occurred despite some substrates offering better matches to other crystallographic orientations [5]. The surface morphology of higher structurally oriented crystals yielded smoother film surfaces, consistent with the general trend that film quality is strongly correlated with lattice mismatch of the film to

the substrate. A 1.0 nm mean roughness value for CdTe:Ge films on sapphire substrates, as measured by atomic force microscopy (AFM), was the most smooth surface achieved and corresponded with the lowest θ-2θ FWHM.

Deposition on $SrTiO_3$ (100) illustrated a key nature of the heteroepitaxial relationship between thin CdTe:Ge on the oxide substrates in that even though there is a better lattice mismatch when compared to sapphire, 1.7% versus 3.7% respectively, when the six-fold symmetric CdTe (111) plane forms an interface with the fourfold symmetric $SrTiO_3$ (100) there are four unique triangular orientations of the (111) plane. For the hexagonally symmetric c-plane sapphire surface there exist only two unique (111) plane orientations. As such, the texture analysis of CdTe:Ge on $SrTiO_3$ (100) and Al_2O_3 (0001) demonstrated the presence of 12 and three additional peaks to the central [111] peak respectively as seen in Figure 5 [5].

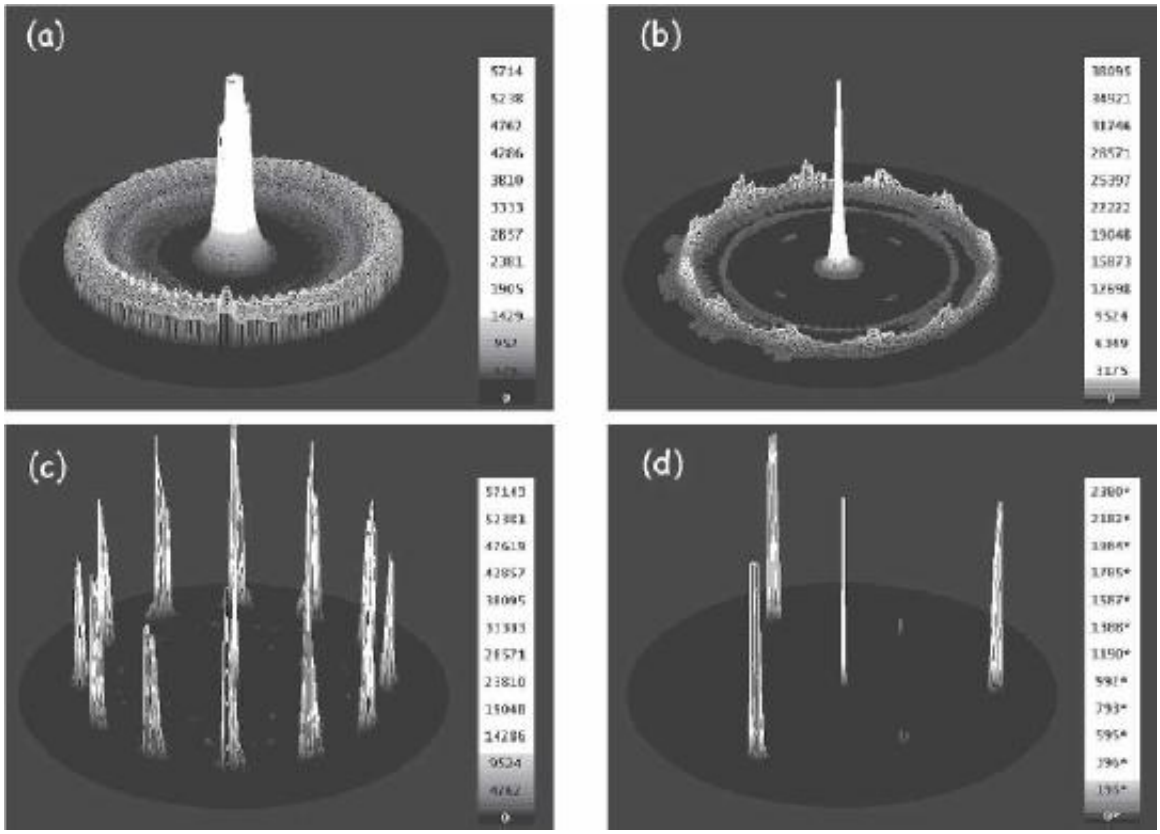

Figure 5: [111] Pole Figures for CdTe:Ge Films Deposited on (a) SiO2, (b) Yttria Stabilized Zirconia (100), (c) $SrTiO_3$ (100) and (d) Al_2O_3 (0001), Modified from [5]

CdTe:Ge film quality had strong correlation to both the degree of lattice mismatch and in-plane alignment of the [111] grains offered by the substrate. Therefore, the most promising substrate for ideal undoped CdTe growth from a pressed powder using PLD in this deposition system is Al_2O_3 (0001).

1.4.2 The Role of Substrate Surface Termination

Evident from the work on the deposition of CdTe:Ge on a variety of oxide crystalline substrates by PLD, both the lattice mismatch and the symmetry of the hexagonal (0001) planes of sapphire make it an ideal substrate candidate for the deposition of CdTe (111)

films. The reduction in the number of domains has been shown to lead to superior quality (111) CdTe films. While there are a wide variety of film qualities reported by several groups, the routine deposition of nearly single domain CdTe (111) on as-received c-plane sapphire substrates by PLD is possible [30]. While texture analysis revealed the orientation of the CdTe (111) domains relative to the sapphire, it was still unclear whether the substrate termination was aluminum, oxygen or a combination of the two. Further, since the CdTe has tetrahedral coordinated Cd and Te atoms the polarity of the films was unknown.

Following the deposition of a gradient of aluminum over the surface of the substrate prior CdTe:Ge deposition a morphological characterization of the film was conducted. Following the gradient of Aluminum across the surface of sapphire it was found that there was a reversal of the CdTe (111) domain by 180°. With a domain selection sensitive to the surface termination of sapphire, it was proposed that variations in reported film quality between groups may be due to different thermal cleaning cycles in different ambient atmospheres prior CdTe deposition [44]. While the termination of the as-received substrate was never measured, it was speculated that it is not aluminum terminated since it would oxidize quickly at the base pressure of the growth chamber.

Polarity analysis was conducted on single crystal films by comparing scanning tunneling electron microscopy (STEM) intensities, which are proportional to the z-number squared, and 2D-XRD pole figures. For the STEM image viewed along the

$[01\bar{1}]$, the Z number intensity profile indicated that the films were Cd-up, (111)A, represented schematically in Figure 6.

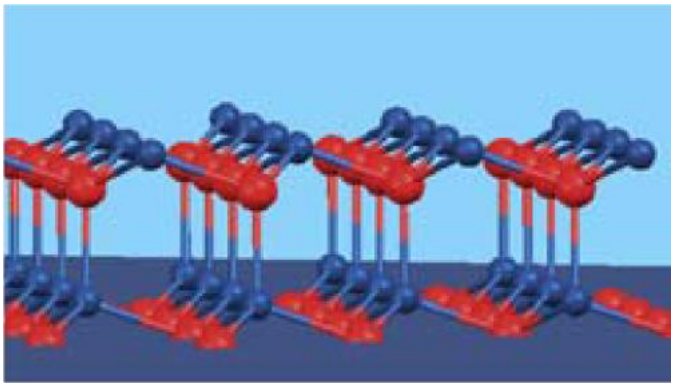

Figure 6: A CdTe (111)A Ball and Stick Model, Modified from [44]

The deposition of CdTe:Ge on as-received Al_2O_3 (0001) substrates by PLD indicated that there is a preference to grow (111)A films. Since geometrically the two CdTe (111) fits to c-plane sapphire are equivalent, the surface termination of the as-received substrates must present an energetic preference for a tellurium initiating layer compared with cadmium in order to achieve single crystalline films. While Neretina et al. suggested that sapphire was either singly terminated by oxygen or aluminum [44], it has been shown c-plane sapphire has three terminations: the stoichiometric (1-Al-terminated), oxygen rich and the aluminum rich (2-Al-terminated); the stoichiometric surface is the lower energy surface relative to the other two [45]. Since germanium substitutes for Cd in the CdTe [46] and its concentration is much less than 1%, it is not anticipated that the orientation or polarity of undoped CdTe films grown from pressed powdered targets will be different than those grown from CdTe:Ge single crystal targets.

Chapter 2 - Equipment and Methodologies

2.1 Deposition and Vacuum Systems

Pulsed laser deposition is a physical deposition technique where a high power laser focused onto a material is used to ablate that material's surface to create a plasma plume. The ejected plasma from the target travels in a medium, such as vacuum or a gas, to a substrate where it condenses and grows as a thin film. The major advantage of PLD to other physical deposition techniques is its ability to maintain stoichiometry between the target and film because of its low mass dependence, medium dependence and confined plasma ejection, unlike techniques such as pulsed electron deposition or sputtering [47].

The process of PLD can be broken down into five overarching steps: laser absorption, plasma creation, dynamic plasma expansion, plasma condensation and film growth. The laser incident on the target material penetrates into the surface with a depth dependent on the laser wavelength and material's attenuation coefficient. For an excimer laser of wavelength 248nm and CdTe this depth is less than 10 nm [48]. The pulse width of the laser must be sufficiently short so that the thermal profile related to the excitation is confined to the excited volume. The excitation of the electrons results in the dissociation of bonds between constituent atoms [49], the formation of ions and the rapid increase in the temperature of the volume to temperatures greater than 7000K [50].

By Coulombic repulsion or thermal expansion, the plasma recoils from the target perpendicularly, reaching supersonic speeds [51]. While spatially the plume has

dependence on the medium in which it is traveling, the density of ions is well described by $cos^n(x)$ function. Depending on the medium of transport, particularly the cross section of interaction and pressure, the plume which was initially narrow and perpendicular to the target surface in vacuum can undergo scattering and diffusion effects. As such, the background pressure and type of gas can be used to lower the spread, deposition rate and average energy of the plume.

When a high energy plume comes into contact with the substrate or film it may sputter atoms off the surface. While this can cause defect formation in the film, sputtered material also serves as a condensation mechanism for the plasma [52]. When the plasma condenses it cools and nucleates in a local minimum energy position. Additional heating of the substrate is used to promote nucleation and growth into energy minimized positions that lead to good crystalline quality. The nucleation density per pulse is high for PLD compared to other deposition techniques and can be advantageous in reducing vacancies and vacancy complexes. A film grows from the condensate by methods such as layer-by-layer, step-flow, columnar and cluster assembly depending on the growth parameters, target material and substrate.

The chamber used to deposit CdTe films is depicted schematically in Figure 7. The films were deposited on as-received diced squares Al_2O_3 (0001) obtained from the MTI Corporation following a cleaning treatment which will be described in later sections. A Light Machinery IPEX-848 KrF with Neon buffer excimer laser, wavelength 248 nm, with beam size 12 mm by 26 mm was masked with a 15 mm by 6.3 mm copper sheet

rectangular aperture to act as the ablation source. The specified maximum stabilized energy output of the laser is 400 mJ per pulse. The energy of the beam across its full shape has a Gaussian profile, thus, while masking the beam allowed for the downshifting of the minimum delivered energy it also improved uniformity of the beam.

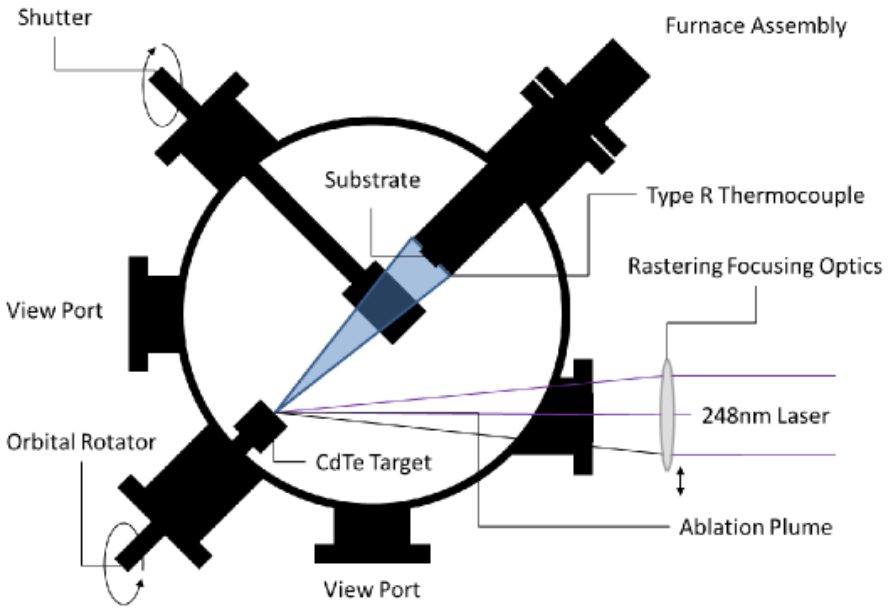

Figure 7: A Schematic Representation of the Pulse Laser Deposition System

The laser has an internal energy monitor. In addition, the energy of the masked beam is measured using an external calorimetric based Scientech 365 power and energy meter. The beam travelling in free space is reflected off a series of excimer laser mirrors, dielectric coated UV grade fused silica, and enters the growth chamber through an excimer laser focusing lens perpendicular to the entry port, a UV grade fused silica window. As indicated in Figure 7, the focusing lens is rastered so that the laser moves radially along the target, prevents trenching and improves the uniformity of the deposited film. This rastering is limited to a 4 mm radial translation from target centre, on a 1 inch

target, inside the chamber because of geometric interference with the target holder. The CdTe target is mounted onto an orbital style rotator, such that the three rotating targets can be rotated about a central axis during deposition to provide three different material sources for growth. A shutter, composed of a Pt coated Incoloy sheet, is used to block the plume's trajectory from the substrate. The plume travels through the transport medium from the target to a heater assembly face where the substrates are mounted. The heater face is Pt coated Incoloy. A cartridge heater, internal to the heater assembly, heats the face where the substrate is mounted through the Incoloy. As such, the heater is separated from the transport medium.

While most depositions of CdTe are carried out in vacuum, the growth chamber is designed to operate in a variety of partial pressures of gas mediums as well. Figure 8 illustrates the pneumatic schematic of the growth chamber. Two pressure gauges monitor the pressure of the chamber. A Granville Phillips 275 Convectron Gauge Vacuum for ranges 760 Torr to 1 mTorr and a Varian SenTorr Gauge Controller for a hot cathode, for ranges 1 mTorr to base pressure. Rough vacuum is achieved in the chamber with a scroll pump. Once a rough vacuum of ~200 mTorr is achieved, the scroll pump is used to back a turbomolecular pump which brings the chamber to a vacuum of ~2E-7 Torr. Using a cold jacket reservoir for liquid nitrogen (LN_2), a base pressure for the system of ~8E-8 Torr can be achieved. This minimum pressure is limited by the use of Viton O-rings and gaskets in the chamber.

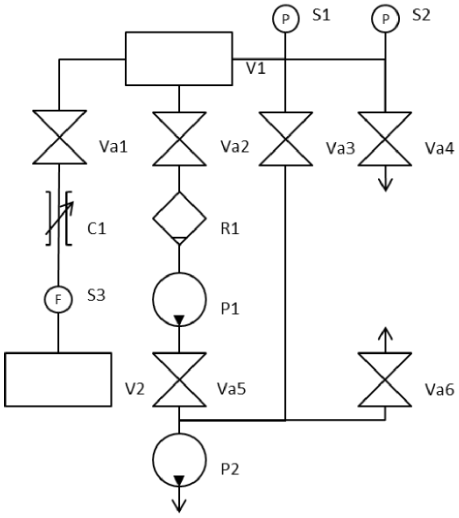

Component Value	Component Name
C1	Granville-Phillips 216 Pressure/Flow Controller
P1	Varian Turbomolecular Pump [Turbo-V 301-AG]
P2	Varian Scroll Vacuum Pump [SH-110]
R1	Cold Jacket Reservoir
S1	Granville-Phillips 275 Convectron Gauge [N_2 Calibrated]
S2	Varian SenTorr Gauge Controller and Hot Cathode [BA]
S3	Sierra Top Trak 821 Mass Flow Meter [He_2 Calibrated]
V1	Chamber Volume
V2	Gas Source [He_2, O_2, Ar_2, and N_2 gas cylinders]
Va1	Gas Shutoff Valve
Va2	Main Pump Butterfly Valve
Va3	Roughing Speedivalve
Va4	Atmosphere Bleed Valve
Va5	Backing Speedivalve
Va6	Scroll Purge Speedivalve

Figure 8: Pneumatic Schematic of the Pulse Laser Deposition Growth Chamber and Legend

With the butterfly valve to the turbomolecular pump partially closed, gas can be introduced to the growth chamber at constant pressure, controlled by Granville-Phillips 216 Pressure/Flow Controller. Flow can be adjusted by acute changes to the main chamber butterfly valve and monitored on a Sierra Top Trak 821 mass flow meter.

The variable growth parameters in the system are the laser energy density, laser repetition rate, growth medium, target-substrate distance, substrate temperature and number of pulses delivered. For the optimization of CdTe undoped films deposited on sapphire (0001) substrates the target-substrate distance was held constant at a spacing

which provides uniform deposition over the substrate's surface. Deposition occurred at the obtainable base vacuum pressure in the system. The two major controllable parameters can be summarized as the plume flux, modified by combinations of changing the laser energy, spot size and repetition rate, and the substrate temperature, which is held constant during growth. As there is no furnace cooler, when growth was terminated the heater relaxed back to room temperature under vacuum at an exponential cooling rate.

2.2 Substrate and Target Preparation

The c-plane sapphire substrates, one and two side polished, were diced in-house with a Microace 3 dicing saw, using a diamond blade, into 12 mm by 12 mm squares. Since the dicing procedure involved the use of a cutting fluid, the substrate surfaces needed to be degreased and cleaned of sapphire debris. The degreasing procedure involves manual irrigation using three solvents, isopropanol, methanol and acetone, such as flushing and wiping with foam tip swabs followed by sonication. A detailed standard operating procedure can be found in Appendix B. Following degreasing, substrates were plasma cleaned in a Solarus Model 950 plasma cleaner, on a Pyrex platform, using the machine's standard H_2/O_2 plasma SEM sample preparation recipe to remove hydrocarbons. These substrates were then mounted to the chamber furnace face where a dry N_2 gun removed any remaining debris before loading. Samples were degassed at 450°C for one hour before deposition to improve the cleanliness of the surface.

Study of the effectiveness of the plasma cleaning and degassing of the substrate have revealed that while they are not necessary to achieve high structural quality films, they

improve the variance in sample quality over repeated experiments. The polished face of an as-received c-plane sapphire substrate is known to present a (1x1) face [53] with a variety of high temperature, >1000°C, reconstructions possible in oxygen rich or deficient atmospheres [54]. Substrate surface preparation should avoid techniques which could cause surface reconstruction. Epitaxial processes have substrate surface dependence by nature. Since the consistency of the substrate surface for growth was not studied, its modification by techniques such as off-cutting, nitration or reconstruction was avoided.

Unlike group IV and III-V semiconductor materials, CdTe and some other II-VI semiconductors remain semiconducting into their liquidus state [55]. Metallic bonds are highly delocalized and so for metals there is a rapid transfer of excess energy to the lattice during laser ablation. Ablation processes in the nanosecond range are normally resisted by metals leading to thermal behaviours instead of plasma ejection. A plasma plume can be achieved for a pulse of high enough energy density [56]. The result of this is that CdTe is an ideal candidate for PLD processes having an ablation threshold of 7.4 mJ/cm^2 with a KrF laser at 1 atm [57]. Achieving a high ionization and atomic degree of ablation specie is easily accomplished in the system and favourable for high quality film deposition [58].

Prior any deposition, the 5N CdTe undoped target, purchased from Kurt J. Lester, was abrasively smoothed each time using Emery paper to remove the influence of macroscopic surface defects in laser interaction, such as trenches, which could block the plume ejection. While previous CdTe:Ge targets were single crystalline, the undoped pressed powder targets used in these experiments could contain voids and required

localized re-melting of the ablation surface before growth. This reduces the ejection of nano-clustered material which could interfere with film heteroepitaxy. It is achieved by striking the rotating target at 2 Hz over the rastered range for a minimum of four minutes, or 480 laser pulses, with the substrate shield in place before beginning film deposition.

2.3 Measurement Systems

2.3.1 Texture Analysis

Obtaining structural information in regards to film quality is an important basis for the quantization of film quality as a whole and can be obtained from x-ray diffraction. In the reflection geometry, the Bragg geometry, elastic scattering from a regular array of periodic atoms by x-rays results in a diffraction pattern with maxima and minima related to the constructive and destructive interference respectively given by Bragg's law in Equation 3:

$$2dsin\theta = n\lambda \qquad \textbf{Equation 3}$$

For a monochromatic x-ray beam with incident angle θ to the surface normal and a periodic arrangement of atoms of spacing d, the beam will be deflected by an angle θ for an inter multiple n of the x-ray wavelength λ. This is depicted in Figure 9.

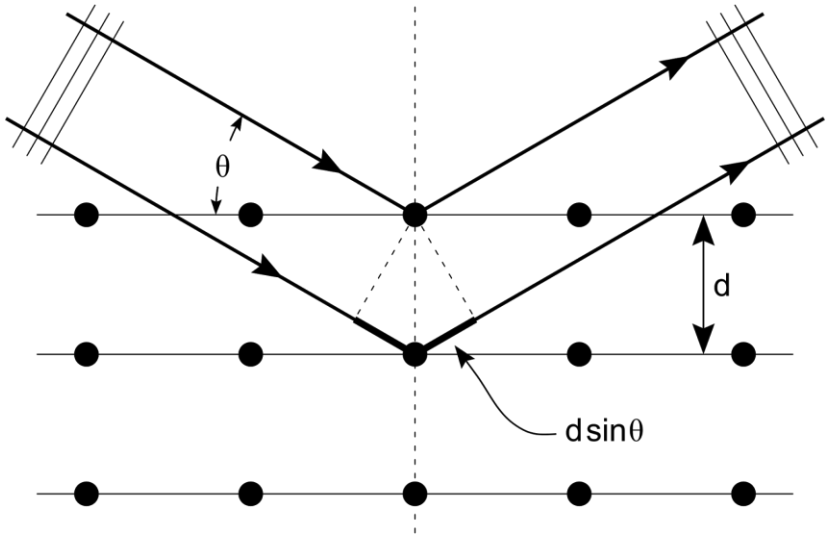

Figure 9: Schematic of the Bragg Diffraction Condition for a Periodic Crystal Lattice

For a θ-2θ diffraction measurement, Figure 9 depicts that the obtained structural parameters are only for lattice parameters perpendicular to the surface. The x-ray point detector relative to the motion of the x-ray source follows a path well defined to look at the widest range of d-spacings possible. For polycrystalline samples, where multiple d-spacings exist along the x-ray source/detector path, crystal structure can be obtained for this method. However, for samples where the lattice spacing differs in periodicity in other directions normal to the surface another method is necessary. One such method is texture analysis; another is x-ray topography.

While the use of texture analysis as an x-ray diffraction technique is not new, the introduction of charge coupled device detectors (CCD) and improvements to computing speed have led to much improved collection and analysis times. A cubic structure with its [100] normal to the surface of the sample, due to cubic symmetry, has periodicities

corresponding to the a-axis given by the family of indices {100}: (010), (001), (-100), (0-10) and (00-1). As such, crystallographic texture merely describes the distribution of crystallographic orientations within a material and can vary from completely amorphous with no orientation preference (isotropic) to single crystalline with one dominant orientation preference (anisotropic).

2DXRD experiments were run using a Bruker SMART6000 CCD on a Bruker 3-circle D8 goniometer with a Rigaku RU-200 rotating anode x-ray generator and parallel focusing mirror optics. The x-ray source was the Cu $k_{\alpha\text{-avg}}$ peak, the average of the $k_{\alpha 1}$ and $k_{\alpha 2}$. A standard experimental run consisted of taking two sets of ten second frames acquired in 2° intervals: a 360° φ-axis scan at ω = -193° and a 60° φ-axis scan at ω = -186°. The values φ, ω and θ describes the Euler angles representing the orientation of a three dimensional object in Euclidean space.

Some experimental runs used finer or coarser frame spacing or longer or shorter acquisition time depending on the sample. The sampling range of reciprocal space was consistent. The surface of the sample is placed at the optical center of the diffractometer. Enough information is provided from the top hemisphere to generate a stereographic projection of the plane defined by the samples surface. For the case of CdTe (111) films deposited on sapphire, the central peak of this pole figure corresponds to the (111) planes being parallel to the substrates surface, while peaks at the edge corresponds to the (111) planes being perpendicular.

2.3.2 Photoluminescence Spectroscopy

In a pure intrinsic semiconductor the primary electronic excitation is the free electron-hole pair, which can be created optically by an absorbed photon with energy greater than or equal to the bandgap energy. While the excited electron may initially be 'hot', it quickly thermalizes to the band edge on a time scale of 10 ps. Due to Coulombic attraction, the associated electron and hole form an exciton. The bound electron-hole pair does not represent two independent quasi-particles but rather a new quasi-particle with internal energy equal to the band gap energy minus the electron-hole binding energy. There exist two basic types of excitons: the Frenkel exciton and the Wannier-Mott exciton [59]. A Frenkel exciton has a small radius, approximately the spatial extent of a unit cell, and is normally found in molecular crystals. The electron-hole pairs constituting Wannier-Mott exciton are separated over many lattice contacts and have a strongly delocalized wavefunction. These excitons occur mainly in semiconductors and move freely about inside the crystal. While free excitons can transfer energy they are electrically neutral and cannot transport charge.

At room temperature the binding energy of excitons is so small they can easily dissociate and recombine. This is called a direct recombination and at room temperature is the dominant photoluminescence (PL) spectrum feature [60]. Radiative, trap-assisted recombination, and non-radiative, Auger recombination, quench band-to-band radiative recombination features in PL spectra. In the case the sample temperature is lowered, PL spectral contributions from defects can be investigated. Shallow neutral or ionized, donor or acceptor states in the semiconductor forbidden zone are caused by extrinsic or intrinsic

defect states in a semiconductor. Excitons can become bound to these defect states Coloumbically and recombine radiatively producing a photon of characteristically lower energy dependent upon the position of the donor or acceptor transition energy level. Emissions from excitons bound to neutral donors and acceptors are designated D^0X and A^0X, while emissions from excitons bound to ionized donors and acceptors are designated D^+X and A^-X respectively. In the case that a free electron-hole pair recombines through impurity states it is called a donor-acceptor pair (DAP) transition. These transitions have lower energy than bound excitons. Below these in energy are deep defects in the forbidden energy region caused by deep point defect states or extended crystallographic defects. Such expected radiative transitions contribution to the PL spectrum as schematically illustrated in Figure 10.

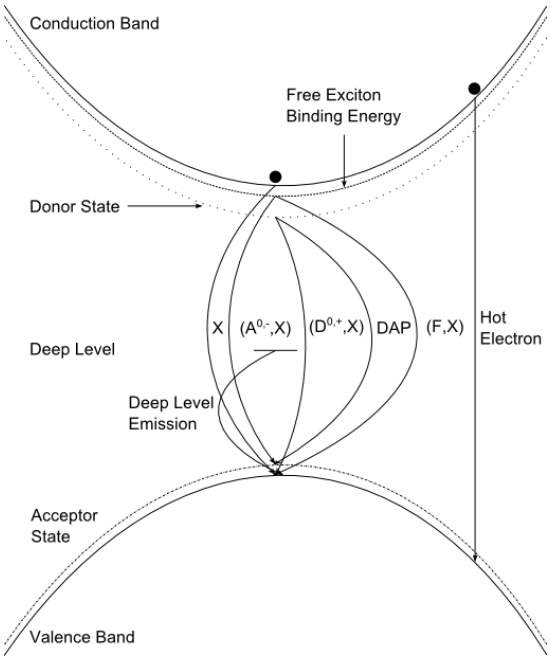

Figure 10: Schematic Representation of Possible Radiative Recombination Mechanisms Contributing to PL Observations at Low Temperatures, Modified from [61]

The line shapes for PL emissions are determined by the probabilistic nature of spontaneous emission, the recombination lifetime of the defect and the material phonon spectrum. To the first approximation, PL emission is expected to be Lorentzian for the system obeying Fermi-Dirac statistics and Gaussian in the case of inhomogeneous broadening by defects [61].

Transitions responsible for the above PL peaks can also be phonon replicas, which occur when the recombination of an electron and hole also involve one or greater lattice phonons causing a characteristic peak shift by an integer number times the characteristic phonon energy. The energy not radiatively emitted is delivered to the lattice. The coupling of photons and phonons in a material is described by the Huang-Rees parameter [62]. For CdTe radiative recombination processes do not involve a strong change in phonon wavevector. Therefore the optical branch of phonons, those which have non-zero energies as their wavelength approaches zero, have the strongest photon-phonon coupling probability. The intensity and shape of the emission lines with phonon participation, seen in Equation 4, reflects the Maxwell-Boltzmann distribution of a free exciton with non-zero kinetic energy, modified slightly to include the probability of phonon creation. Equation 4 was modified from [59]:

$$I(x) \approx \left(x - \left[E_g - E_X\right] - n\hbar\omega_0\right)^{\frac{3}{2}} exp\left(-\frac{x-\left[E_g-E_X\right]-n\hbar\omega_0}{k_B T}\right) \qquad \textbf{Equation 4}$$

Where E_g is the energy of the bandgap, E_x is the energy of the excitonic radiative emission and $n\hbar\omega_0$ is the energy lost to the lattice from multiple optical phonons (LO phonons). It is common to describe direct radiative recombination about the critical point

as Lorentzian and Gaussian for excitonic recombination. The temperature dependence of excitonic PL emission reveals information about the activation energy responsible for the specific recombination feature. The effect of the density of states on the free exciton contribution to the PL spectrum for bulk CdTe has been experimentally determined [63]. Neglecting the temperature dependence of the exciton binding energy, fitting to the peak position of a PL emission below the band edge in an Arrhenius plot reveals the activation energy of the recombination centre and information about the excitonic population.

PL was measured using a 0.55 m Horiba Jobin Yvon spectrometer and dispersed onto a LN_2 cooled Silicon charge coupled array. Light collection from the film was achieved using a microscope with 60x objective with a numerical aperture of 0.004. A 130mW Argon Ion laser, 488 nm, or a 320 W/cm^2 He-Ne laser, 632.8 nm, were the two possible excitation sources focused to a spot size of 2 μm through the microscope objective. Normally the Argon ion laser was used because of its higher intensity. Low temperature PL was also taken using an open-cycle Helium cryostat in the range of 10K to room temperature.

2.3.3 Photoreflectance Modulation Spectroscopy

In experimental physics the measurement of a parameter from a spectrum is sometimes difficult because of the magnitude of its contribution to that spectrum relative to other parameters. Instead by measuring the partial derivative of that spectrum with respect to a variable in which only the parameter of interest is not constant, the parameter can be precisely extracted. Photoreflectance (PR) modulation spectroscopy involves the optical

perturbation of a sample's internal electric fields by a pulsed excitation source of known periodicity. A sample's reflectance spectrum is measured continuously via DC coupling. A laser beam is absorbed in the semiconducting material and generates electron-hole pairs that alter the complex dielectric function. The complex dielectric function is altered because an electron-hole pair dissociates under the influence the sample's internal or surface field, reducing that field. A chopper modulates the laser so this effect is modulated and a lock-in amplifier via AC coupling measures the modulated reflection spectrum. The ratio of the modulated reflection spectrum to the DC reflection spectrum gives rise to a derivative spectrum in regions where optical recombination processes occur. The derivative nature of the measurement produces sharp spectral features which are observable even at room temperature. Further, with phase sensitive analysis even smaller changes in the reflectance spectra can be resolved. Fundamental experimental and theoretical work in the area of PR methods provides the framework for the development of analysis techniques sensitive to within a few meV [64].

An example of internal electric field modulation is depicted in Figure 11. At the surface of a semiconductor the Fermi energy is pinned because of the surface states creating a space charge region. This can be modulated with an optical pulse. Other electric fields may be present in a sample as well when the sample is not illuminated [65].

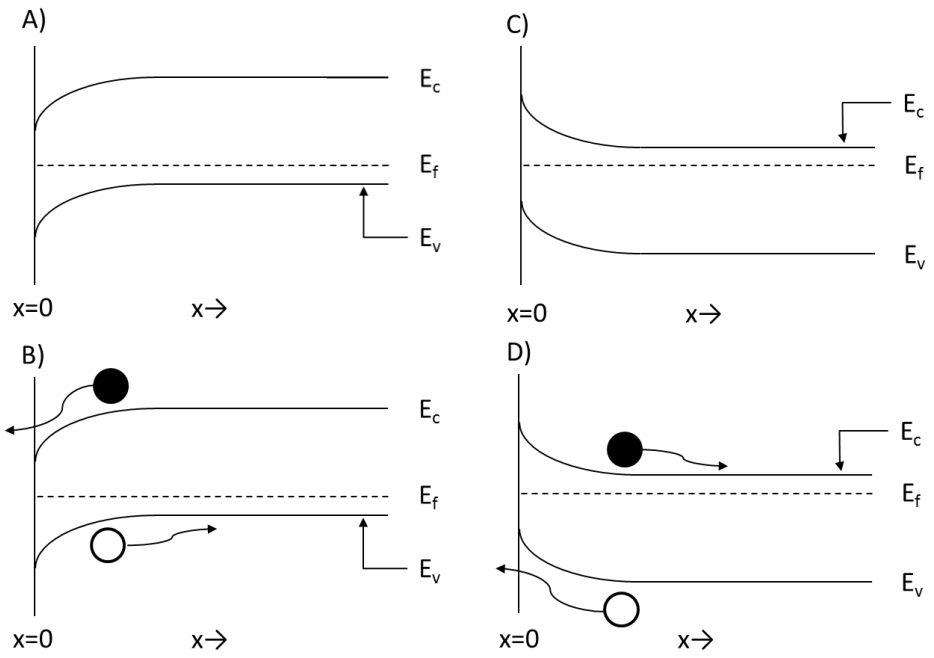

Figure 11: Schematic Representation of Photoreflectance Effect in A) p-type sample in the dark E_f pinned as surface B) Photoexcited carriers separate and minority electrons neutralize charge in surface states C) n-type sample in the dark E_f pinned as surface B) Photoexcited carriers separate and minority hole neutralize charge in surface states

Using an optical chopper to modulate a laser beam with energy above the band gap of CdTe, a photoinduced variation of the electric field at the surface is created as well as a signal which can be detected with a lock in amplifier. The base reflection spectrum for the sample being modulated, the DC signal, is created by a broad light source reflected off the sample. The DC signal is collected together with the AC signal using a detector and monochromator so that the modulated spectrum can be normalized to the DC spectrum.

Since surface states contain electrons or holes from the bulk for an n-type and p-type semiconductor respectively, photoexcited electron-hole pairs are separated and minority carriers are swept towards the surface to neutralize the trapped charge. This reduces the

surface field. The modulated surface field is resolved in the reflection spectra and has been shown to be sensitive to optical point transitions in the Brillouin zone as well as weak features in the absolute reflection spectrum. Sensitive enough to account for line shapes in the modulated spectrum [66].

Differential changes in the reflectivity are related to the perturbation of the complex dielectric function and can be classified into low field and high field regimes depending on the relative strength of characteristic energies [64]. In the low field regime, where the electro-optical energy is less than or equal to the broadening parameter, modulation from already flat bands can be considered [66]. It has been demonstrated that a complex dielectric function with Lorentzian optical resonances adequately describes this regime for semiconductors [67]. Assuming the distribution of states near the critical point has a Lorentzian shape Equation 5 describes the PR spectrum [68]:

$$\frac{\Delta R}{R} = Re\left[Ce^{i\phi}(E - E_g + i\Gamma)^{-m}\right] \qquad \textbf{Equation 5}$$

Where C is the amplitude, Φ is the phase of the complex dielectric function, the influence of non-uniform electric fields or electron-hole interaction effects and E_g is the bandgap energy. For three dimensional critical points, such as the direct bandgap of CdTe, the value of m is 2.5 [67]. Equation 5 can be written in the form of Equation 6 and used for fitting to measured data:

$$\frac{\Delta R}{R} = \frac{C}{\sqrt{\left[\left(E-E_g\right)^2+\Gamma^2\right]^m}} cos\left[\phi - 2 * m * arctan\left(\frac{1}{\sqrt{1+\left(\frac{E-E_g}{\Gamma}\right)^2}} + \left(\frac{E-E_g}{\Gamma}\right)\right)\right] \qquad \textbf{Equation 6}$$

In the case of a Gaussian dispersion near the critical point, such as excitonic behaviour, numerical calculation of the fit can be difficult because of the recursive term, however, an estimate of the Gaussian dispersion can be made with a Lorentzian for which the value of m is unconstrained in fitting [69].

In the high field case the band structure remains unchanged and the reflectance spectrum line shape contains Franz-Keldysh oscillations as described by the condition in Equation 7 [70]:

$$|\hbar\theta| = \left|\sqrt[3]{\frac{q^2\hbar^2E^2}{2\mu}}\right| \geq \Gamma \qquad \textbf{Equation 7}$$

Where ħθ is the electro-optical energy, Γ the broadening parameter, E is the electric field magnitude and μ is the inter-band effective mass in the direction of the internal field being oscillated. Since the high electric field breaks the translational symmetry of the material and causes the acceleration of electrons and holes, separating excitons, it is not appropriate to study near gap transitions. Unlike the perturbation of band bending at surface states which occurs during modulation in the low field regime, tunneling effects from high electric fields may dominate in the high field regime. While it is not expected that the undoped CdTe film on an insulating substrate will be in the high field regime, it is important to distinguish between the two by looking for Franz-Keldysh oscillations in the spectrum.

PR experiments were performed with a Bruker Optics Vertex 80v FTIR with a Silicon detector and a Mercury-arc lamp modulated by a 510 nm diode laser chopped at 210 Hz. The modulated signal was measured using the quadrature component of lock-in amplifier.

Spectra were taken at room temperature under a slight vacuum of 4 Torr. Vacuum PR spectroscopy improves sensitivity of mid to far infrared regions where water vapor absorptions can occur. A schematic of the setup is shown below in Figure 12.

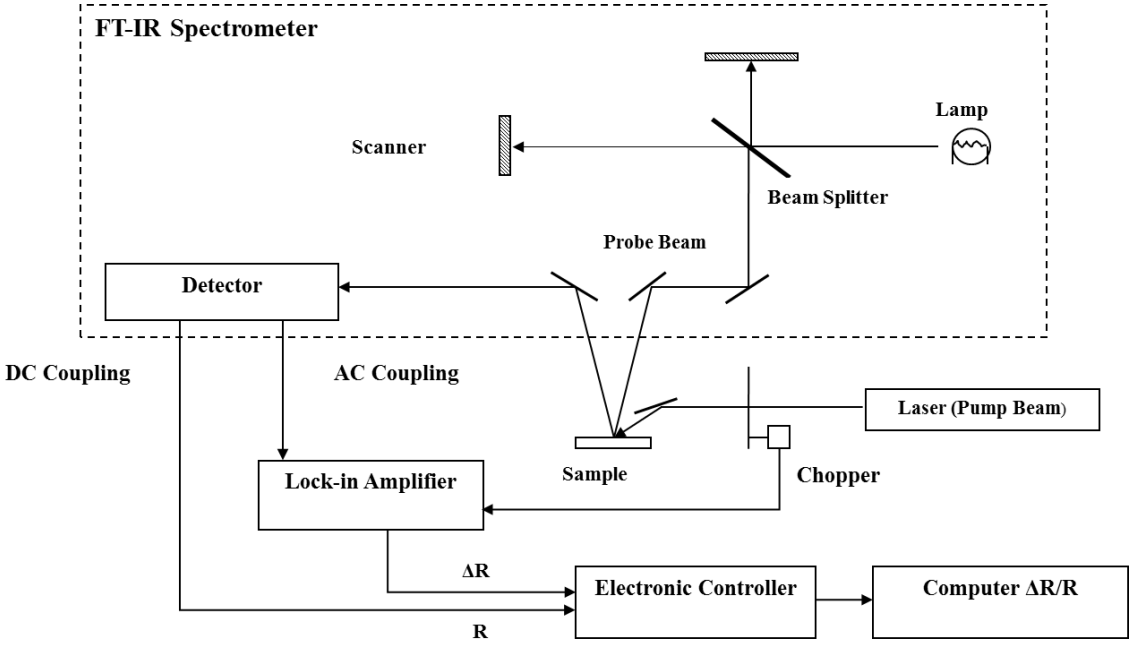

Figure 12: Bruker Optics Vertex 80v FTIR Schematic Setup to Measure Photoreflectance Spectra

Chapter 3 - Results and Discussions

3.1 Structural and Growth Optimizations

Publications of CdTe:Ge film growth on c-plane sapphire via PLD using crystalline CdTe:Ge targets provided the starting growth conditions for the optimization process using undoped pressed powder targets; a laser energy density of 2 J/cm^2 with rectangular image size of 4.5 mm^2 at a repetition rate of 8 to 10 Hz onto a substrate at a temperature of 300 to 310°C in high vacuum [44], [5]. The measured target-substrate spacing was 34.00±0.02 mm. In order to confirm the focal length of the lens and image size of the masked laser beam pattern onto the target, single laser shots were fired and then residual pattern was measured using optical microscopy image analysis. The magnification coefficient was determined by dividing the measured image size by the masked beam size of 15 mm by 6.3 mm. The results are summarized in Figure 13 below.

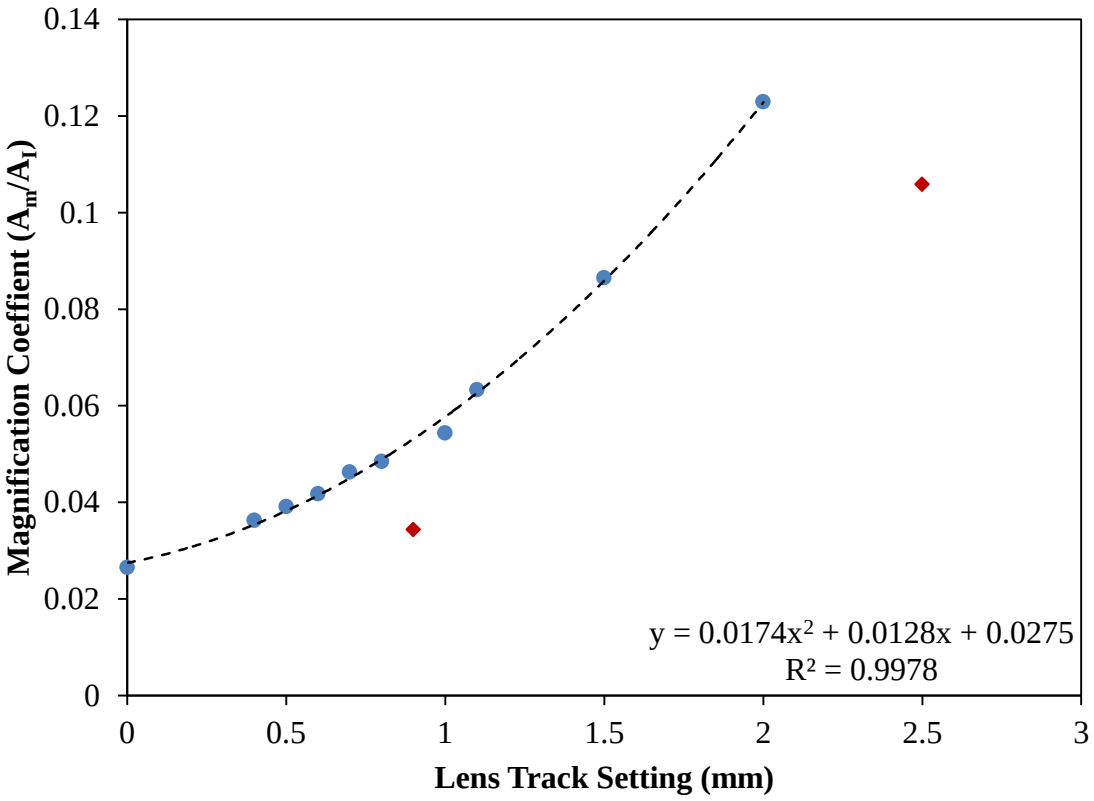

Figure 13: PLD Imaging Lens Calibration Curve with Two Experimental Outliers Marked in Red Representing Laser Misfires Not Included in the Fit

The linear magnification of an object, the ratio of the image size to the object size, for magnifications less than 1 should produce an image that is inverted and related to the ratio of the image distance to the object distance. This rational function is approximated by a quadratic over the lens' track range, as measured on the micrometer of a translating stage. The quadratic provides an excellent fit well over the region of interest. Two outliers were not included because the image quality of their laser mark on the target was distorted indicating that the laser had misfired. The approximate lens position to achieve an image area of 4.5 mm^2 is given by a micrometer reading of 0.77 mm. Since the stabilized laser energy output has a variance of 10%, the accuracy of the micrometer

setting is almost negligible in comparison. Consistency in the system was maintained between growths by keeping the optics static after the initial calibration.

Initial attempts to produce single crystalline undoped CdTe from a pressed powder target, using growth parameters for a CdTe:Ge single crystal target, resulted in un-textured, multiply twinned films. A crystal twin occurs when two separate crystals share the same points of a crystal lattice and intergrow. Twins represent an interruption or change in the lattice sequence. While the interface between the main crystal and its twin is a relatively benign defect, twins can contribute negatively to the electrical properties of semiconductors when their boundaries collide incoherently. Multiple crystalline orientations were noticeable from visual inspection by haze in the films indicating diffuse light scattering. This feature was dominant in the centre of the substrate where the density of the plume was the highest.

The flux of the plume incident on the substrate is modifiable through a variety of growth and system parameters such as the image size, beam energy, target-substrate distance, alignment of plume centre to the substrate and beam repetition rate. It was postulated that after the initial realignment of the PLD system during re-commissioning, the capture rate of the plume onto the substrate was too high relative to previous experiments. The system was previously calibrated to capture the fringe of the ablation plume instead of its centre. While modifications of the growth temperature and laser energy in the beginning appeared to have little effect on the film crystallinity, a reduction

in the repetition rate of the laser had a drastic effect on the film structure as summarized by Figure 14.

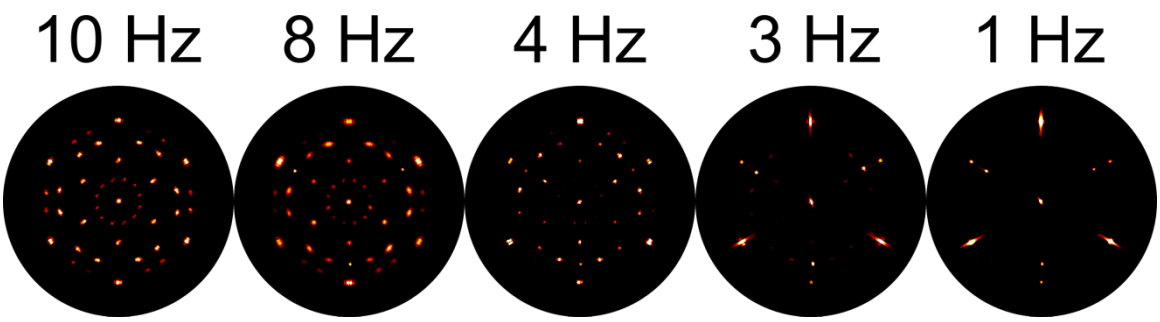

Figure 14: 2DXRD Stereographic (111) Projections of CdTe (111)/Al_2O_3 (0001) Films Grown at Different Laser Repetition Rates for a Target-Substrate Spacing of 3.4 cm

The central peaks in Figure 14 indicate that the films have grown with their (111) planes parallel to the substrate surface. The outer circumference of the pole figure indicates orientations in-plane with the substrate surface. Peaks occurring on other rings indicate orientations with [111] d-spacing rotated out of the substrate surface plane. The three inner ring peaks, seen most clearly in the 1 Hz pole figure but also appearing in other pole figures in Figure 14, are attributed to bleed through of sapphire peaks into the 2θ shell of interest. These peaks combined with the outer ring peaks determine how the CdTe domains are oriented with respect to the sapphire substrate. Single crystal CdTe (111) is represented in a (111) pole figure by three outer ring peaks, either aligned with or rotated 180° to the three inner three sapphire peaks, and one central [111] peak. Additional peaks represent a decrease in texture and therefore crystalline quality.

Peak broadening along the ring in the pole figure indicates in-plane crystallographic misalignment. The radial broadening is consistent with inhomogeneous strain. The measurement of the 2θ values for the {111} indicates that the [111] d-spacing, perpendicular to the substrate, is different than the d-spacings in $[\bar{1}11]$, $[1\bar{1}1]$ and $[11\bar{1}]$, 70.529° from the [111], in the films.

For PLD, the repetition rate of laser pulses is proportional to the film growth rate. As well, the growth rate is predicted to decrease linearly with an increasing growth temperature. (111) pole figures in Figure 14 of CdTe (111)/Al_2O_3 (0001) films have strong (111) orientation with increasing texturing left to right. The film grown at 1 Hz is strongly epitaxially aligned to the substrate with host domain and a first order twin corresponding to a 180° rotation in-plane. The decreased texturing seen in the pole figure for the 3 Hz sample compared to the 1 Hz sample is attributed to second order twinning. A dominant host domain, rotated 180° with respect to the sapphire substrate reference peaks, is maintained in the films up to 4 Hz.

For repetition rates 3 Hz to 10 Hz the decrease in texture and increase in complexity of the pole figures are attributed to further twinning. The symmetry of the most common form of twin, where the boundary lies on a {111} in both the twin and host lattice orientation, is high in CdTe and thus the expected boundary energy is low. There are two possible explanations for the strong texture dependence on growth rate which are not mutually exclusive. Adatoms from the condensing plasma may lack the mobility necessary to find their absolute minimum energy position in the time available between

pulses leading to low energy extended defects such as twins and stacking faults. Recall that the growth temperature range 300°C to 310°C is low relative to the melting point, 1092°C. The second consideration is that the plume is not purely atomic and ionic and it contains nano-clusters either formed in the plasma or that are ejected from the target. These clusters could seed defects if the timescale for annealing is insufficient. The growth rate dependence of texturing and uniformity of the film were addressed simultaneously by increasing the target-substrate.

Equation 8 describes the spatial distribution of the plasma plume thickness [71]:

$$T(x,y) = T_0 cos^m\theta_x cos^n\theta_y \qquad \textbf{Equation 8}$$

where T_0 is the thickness at the centre of the plume, θ_x and θ_y are the angles of divergence from the plume centre and m and n are the power coefficients that describe the rate of decrease in thickness of the film. Defining z as the target-substrate distance, in the axial direction from the target, the angle of divergence is the arctan of the ratio of the radial position along the plume to the distance z. Substituting into the cosine proportionality we can achieve a generalized description of the plume's spatial variance. Assuming the variation in the x and y direction are equivalent, Equation 8 can be rewritten as a function of z and target radius r as Equation 9.

$$T(r,z) \approx [1 + (r/z)^2]^{-\frac{n+3}{2}} \qquad \textbf{Equation 9}$$

The power coefficient must be an integer value greater than one. For the PLD system the best fit value was 12. The film thickness was measured via stylus profilometry. Figure 15 depicts the predicted normalized thickness variation of the plume as a function of the

plume radius for various target-substrate distances, defined as the height in PLD growth geometry.

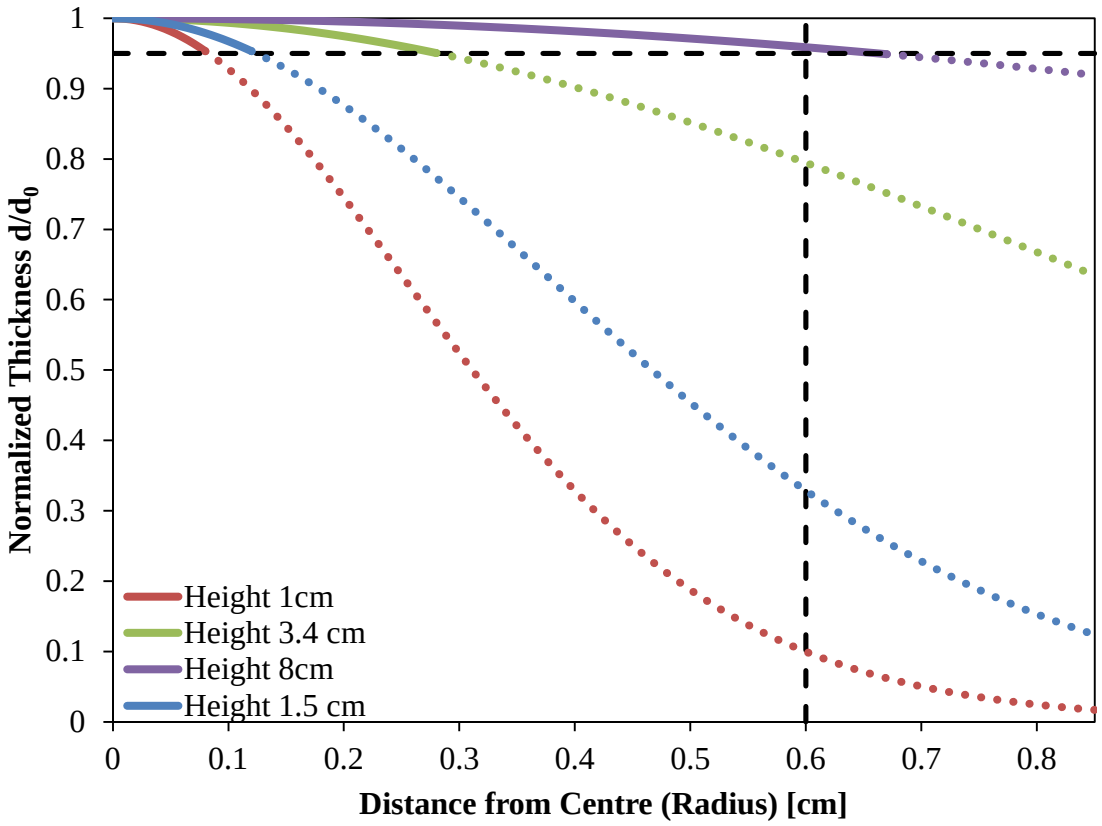

Figure 15: Calculated Normalized Thickness of Sample as a Function of Plume Radius Demonstrating Reasonable Uniformity, 95% of Central Thickness, Out to the Sample Edge at 6 mm from the Centre

The 95th percentile of the normalized thickness is indicated by a horizontal line on the above graphic. Since the extent of laser rastering is approximately 4 mm, further would result in asymmetry because of the line of sight between the target and the substrate, the minimum target-substrate distance which results in a 5% deviation in thickness over the sample is 8 cm. The distance between the target and substrate was increased to 8 cm and the initial growths were repeated in order to observe a predicted increase in texturing.

Growths repeated varying only the repetition rate, other growth parameters were held constant to the parameters used to grow single crystal CdTe:Ge films, ~2 J/cm^2 at 310°C, with the same number of laser pulses yielded significant results summarized below in Figure 16.

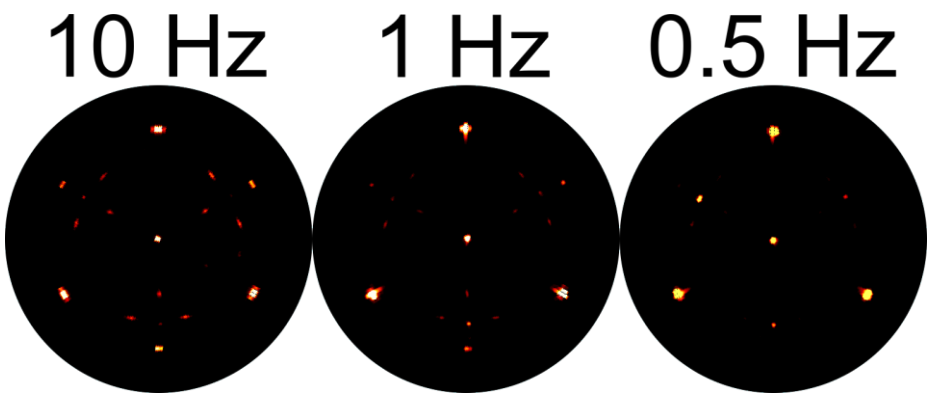

Figure 16: 2DXRD Stereographic (111) Projections of CdTe (111)/Al_2O_3 (0001) Films Grown at Different Laser Repetition Rates for a Target-Substrate Spacing of 8 cm

For the sample grown at 10 Hz, a significant increase in texture when grown at a spacing of 8 cm was noticed. Maintaining the same background levels in all three pole figures, lowering the laser repetition rate to 1 Hz and 0.5 Hz drastically increases the texturing. The results were fractional twinning in the CdTe (111) film grown at a rate of 1 Hz and a single crystalline CdTe (111) film grown at a rate of 0.5 Hz.

It was empirically demonstrated that regardless of the mechanism of texturing at 3.4 cm, as the plume is more uniformly distributed across the 12 mm by 12 mm sample the texturing of the film is increased. While single crystal films were achieved, variation sample to sample was still quite high without a rigorous preparation of the substrate and

target surface. The increase in target-substrate distance improves the uniformity and modifies the plum flux across the sample. With reference to the sapphire substrate bleed through peaks in the (111) pole figure, the undoped CdTe single crystal domains have the same orientation of host domain as CdTe:Ge films grown previously.

At a reduced growth rate and increased target-substrate spacing the growth of undoped single crystal CdTe films on Al_2O_3 (0001) was achieved. The film quality was no longer dominated by the repetition rate but rather the effect of other growth parameters could be investigated and mapped to the PLD process space. This allowed for further insight into film growth and optimization. At a repetition rate of 0.5 Hz and stabilized energy density of 1.78 J/cm^2, samples were grown over the temperature range from 310°C to 200°C. Samples all received the same number of plume pulses, 1800. Integrating around the ring in the (111) pole figure, the x-ray diffraction intensity for the host and first order twin was compared for films. Since the peak height of the x-ray diffraction feature is proportional to the number density of that crystallographic feature, the ratio of the twin peak height to the host peak height is an approximation of the twin density in the film.

Plotting this approximation of the twin density as a function temperature Figure 17 demonstrates a near linear decrease in twin density with increasing temperature.

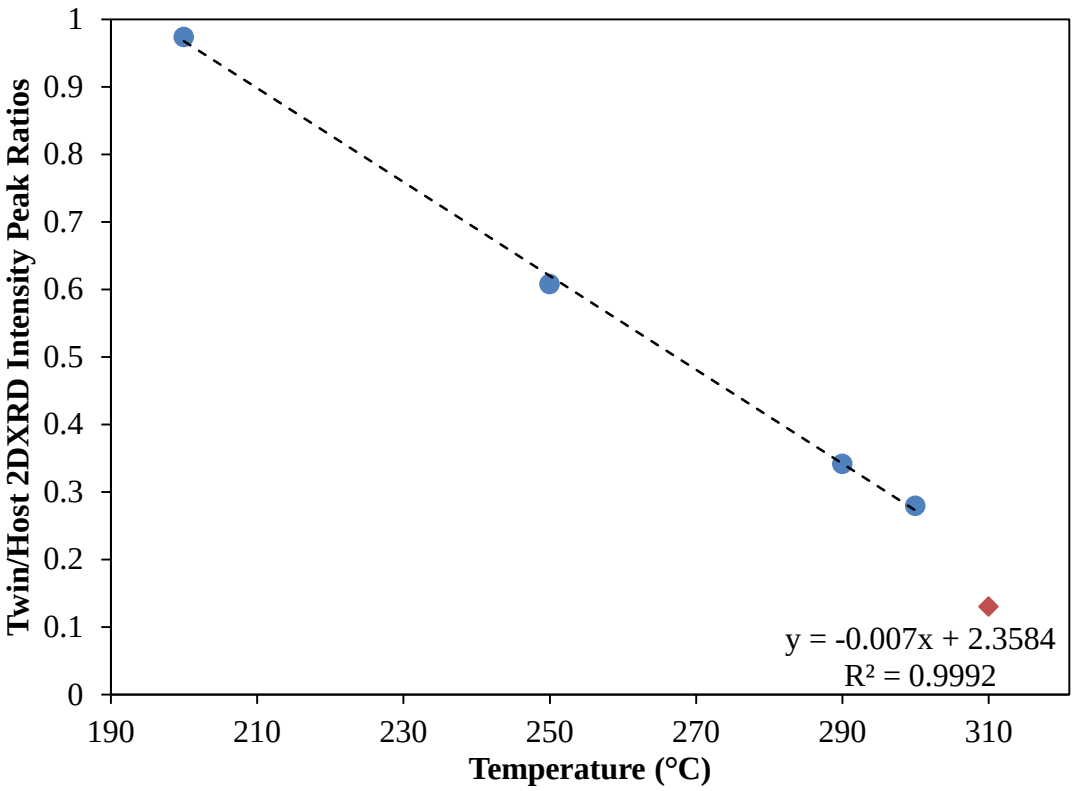

Figure 17: Approximate Twin Density in CdTe (111)/Al_2O_3 (0001) Films as Function of Temperature where Linear Trend Roll-off occurs as Film Sublimation Becomes Significant Compared to the Growth Rate at Higher Temperatures

Two side polished substrates, in strong thermal contact with the furnace, grown at temperatures approaching 321°C films have films which are visibly thinner, in the radial direction of the furnace. Film growth does not occur in these cases over the entire substrate. Films can be grown at increased substrate temperatures by increasing the laser repetition rate, indicating that the film net thickness has temperature dependence. For one side polished samples film growth as a function of temperature, at low laser repetition rates, ceases approximately 10°C higher; it is likely become the unpolished side of the substrate makes poor thermal contact with the furnace. In the literature it has been shown

that the density planar faults and twins decreases as a function of growth temperature for CdTe sublimated films [72]. Yan et al. calculated using first principle total energy calculations, for CdTe, the formation energies for lamella twins, intrinsic stacking faults and extrinsic stacking faults to be 99.9 meV/nm^2, 212 meV/nm^2 and 193 meV/nm^2 respectively [73]. It is postulated that an increase in temperature provides both more energy to adatoms to move into the correct crystallographic positions and decreases the net growth rate through temperature dependent desorption processes.

The thickness of the films grown over a temperature range of 350°C to 200°C was then measured by stylus based profilometry. The films were also measured by broad source optical profilometry and those results agreed with observed stylus base profilometry trends. There was, however, an offset in the optical data accredited to unaccounted thin film effects. An additional sample was grown with the heater off, at a stabilized growth temperature of 28°C, with all other grown parameters the same including the number of plasma pulses. Each sample received 1800±3 pulses and the tolerance of the thermocouple is 1.5°C. An estimate of the sample thickness was made by measuring the same corner of the first quadrant of each sample. Normalizing to the number of delivered pulses an estimate of the delivered thickness per pulse can be plotted, see Figure 18, against sample growth temperature to look at dependencies.

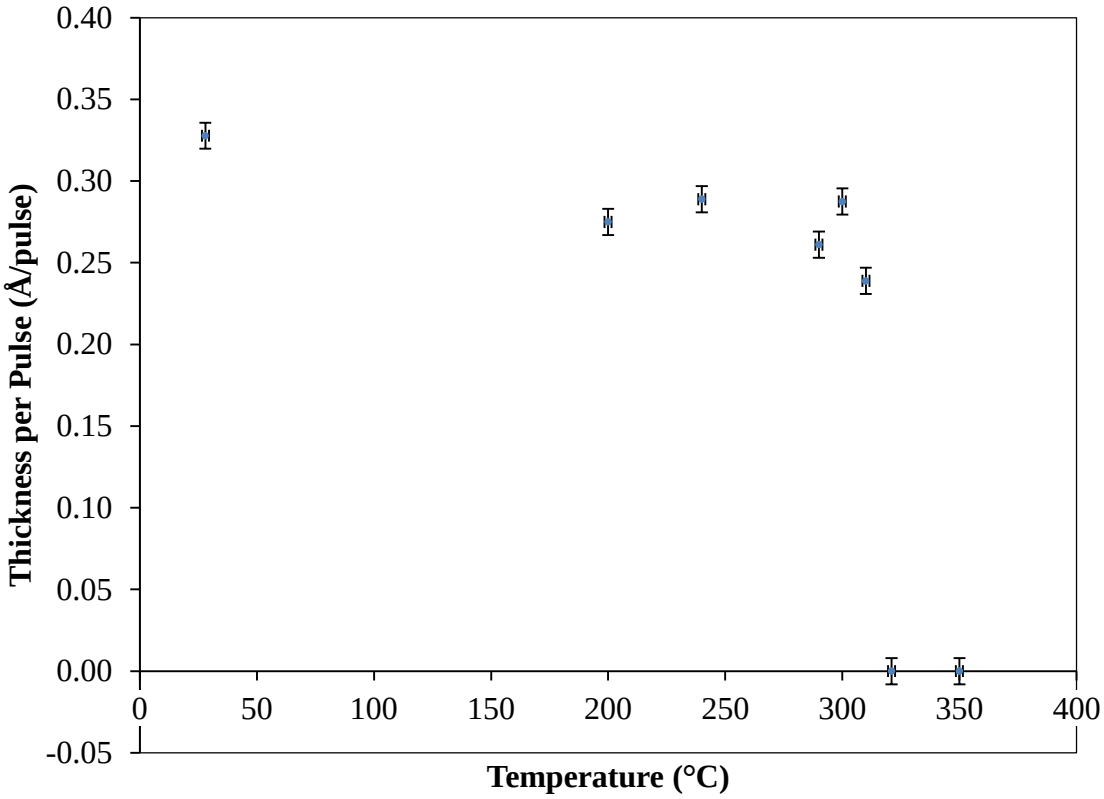

Figure 18: Rate of Thickness Change per Pulse as a Function of Temperature Measured by and Stylus Profilometry for CdTe (111)/Al_2O_3 (0001) Films

A single corner sampling is insufficient to gauge the average thickness of the film. For the case of the 310°C growth, the third quadrant sample corner opposite the thickness measurement did not have any visible trace of CdTe. This indicated that there is non-uniform temperature across the furnace face not reflected in the thermocouple measurement of growth temperature. Upon first glance Figure 18 is not impressive because there is only a weak decreasing trend as the substrate temperature is increased. However, the data spread in the 28°C to 310°C range represents a change in 0.1 Å/pulse over a temperature range of 270°C indicating that at a laser repetition rate of 0.5 Hz there is likely a negligible void fraction in the film even at room temperature. As well, between

the sample grown at 28°C and the one grown at 310°C difference in thickness was only 36 nm.

Certainly a loss of material from the substrate occurs as the furnace is brought to higher temperature, noted repeatedly as a visible change in the samples and in the inability to nucleate films at a pulse rate of 0.5 Hz for temperatures above 321°C. Since the system thermocouple measures the temperature near the outer radius of the furnace to be constant during growth, a gradient in temperature across the face must exist; likely as a function of the heating system itself coming to equilibrium with the vacuum surrounding it. The growth rate, which appears to be less than a monolayer per pulse, appears to be fairly temperature stable over the range of 28°C to 310°C, where significant loss of film growth occurs around 321°C. Insight into the stability of the epitaxial growth and stoichiometry of CdTe films is found in Figure 19, the binary phase diagram of CdTe.

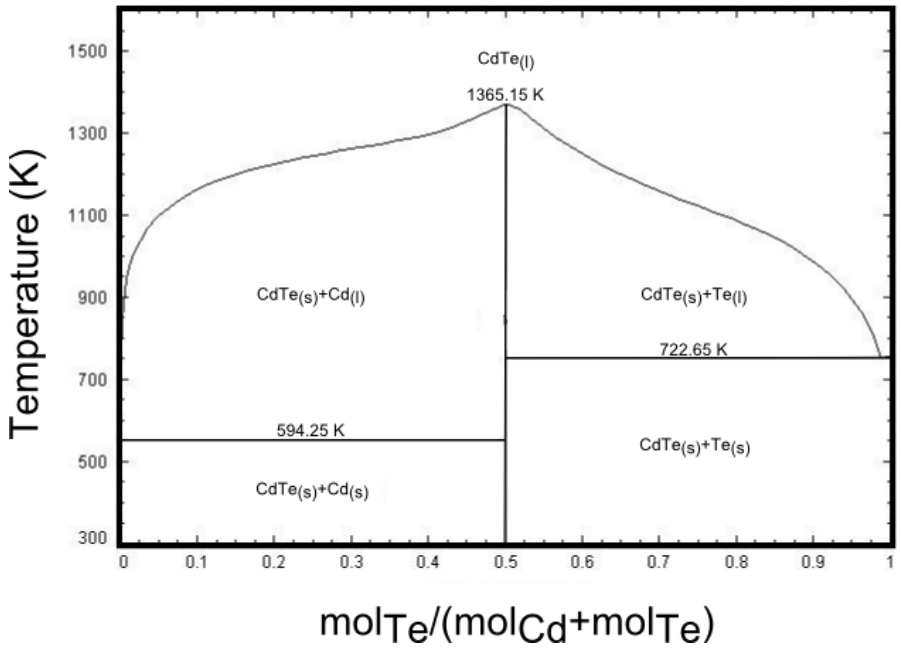

Figure 19: CdTe Binary Phase Diagram, Modified from [74]

The melting point of Cd and Te are about 321°C and 450°C respectively while the melting point of CdTe is 1092°C. The increase in solid stability of CdTe compared to its atomic constitutions implies that the vapour pressure of CdTe from $Cd_{(v)}$ and $Te_{2(v)}$ components is much less than from bulk Cd or Te; at least for growth temperatures less than the liquidus point of excess Cd in CdTe [75]. It is hypothesized that for a CdTe (111)A crystal, in order to maintain a stable surface as part of the Cd surface leaves some Te must also leave; the transverse of this stabilization would occur for a CdTe (111)B film. This could occur by a desorption process like sublimation. For a laser repetition rate of 0.5 Hz it is expected that the net film growth rate is about 0.13 Å/s at 300°C. Since no film grew at this laser repetition rate at 321°C, the desorption rate must at least be equal to or greater than 0.13 Å/s at this temperature; rates of this magnitude are consistent with sublimation experimentation in literature for the (111)A face at 321°C [76].

In addition to studying the effect of temperature on film growth, the effect of film thickness on film quality was studied. For a growth temperature of 300°C, the net growth rate of the film as measured in the centre of the film by variable angle spectroscopic ellipsometry was determined to be 0.33 Å/pulse or 0.165 Å/s. Holding all growth conditions at the optimum setting for texture maximization, samples were grown with 900, 2700, 3600 and 4500 pulses. Figure 20 plots the approximate first order twin density, normalized to the host domain, as a function of thickness. The data if well fit by an inversely proportional square dependence.

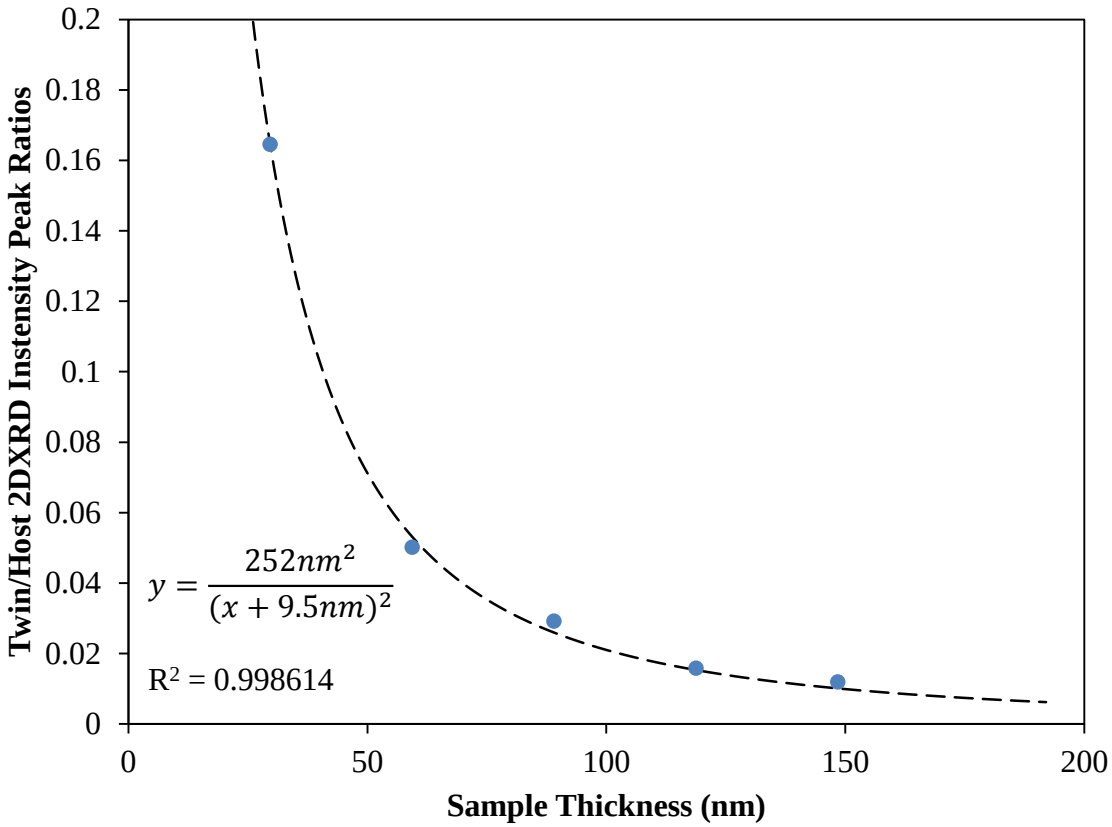

Figure 20: Approximate Twin Density in CdTe (111)/Al_2O_3 (0001) Films as Function of Thickness

As the thickness of the CdTe film increases, texture analysis reveals only a single domain in the diffraction pattern; since the signal for the twin is lost instrument background. Similar inverse squared dependence of epitaxial CdTe film quality has been reported in literature [77], [78]. Whereas misfit at the CdTe (111)/Al_2O_3 (0001) interface causes tensile strain, as the film grows from the substrate it is expected to relax after a critical thickness. The inverse squared dependence of the 1st order twin density is postulated to be caused by a defect or defect network near the interface at the critical thickness; the defect does not propagate through the film such as stacking fault [79]. The calculated y-asymptote of 9.5 nm is indicative of the critical thickness for these films or the point in which single CdTe (111)A growth begins. Without high resolution transmission electron microscopy of the CdTe/sapphire interface, the interfacial defects and the mechanism of strain relaxation cannot be easily identified.

The effect of laser energy density on film quality was briefly studied but there appeared to be no strong sensitivity for values about 2 J/cm^2. At approximately 1.3 J/cm^2 film structural quality did begin to decrease, as evaluated by texture analysis, however, no change in film quality was noted for energy densities about 2 J/cm^2. Since CdTe (111) single crystalline films are obtainable at an energy density of 2 J/cm^2 it is assumed the plume almost purely ionic and atomic in content. The range of energy densities studied did not extend high enough into the non-linear ablation or significant film sputtering regime.

The 2DXRD results for films grown at 2 J/cm^2 with a laser repetition rate of 0.5 Hz at a substrate temperature of 300°C are consistent with high structural quality material. However, the structural analysis yields no information about specific point or complex defects that is important in terms of the electronic quality of the material. The linear and inverse squared relationship of the effect of temperature and thickness respectively on film structural quality was discussed previously. The (111) pole figure of a CdTe (111) film and a CdTe (111) single crystal wafer, purchased from the MTI corporation, are displayed below in Figure 21 for reference of structural quality for the film under optimized conditions.

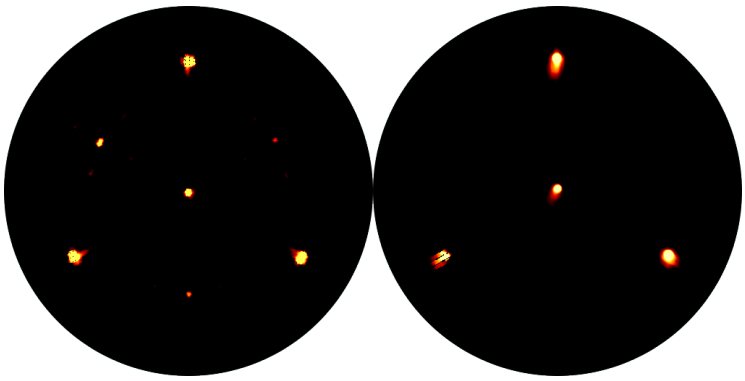

Figure 21: 2DXRD Stereographic (111) Projections of a CdTe (111/)/Al_2O_3 (0001) (Left) and a CdTe (111) Single Crystal Wafer Purchased From MTI (Right)

Both the single crystal wafer and thin film had strong orientation and texturing in the directions perpendicular to the surface. Effectively, the only differences between the texture analysis for the film and wafer are that the sapphire substrate of the film contributes three additional peaks to the pole figure for the film and the diffraction intensity of the wafer is greater than the film. Both of these differences are due to the film

being thin. Essentially the undoped single crystal films are identical to undoped single crystal wafers grown by the Bridgman method with respect to X-ray texture analysis.

3.2 Optical Characterizations

3.2.1 Photoluminescence

For films grown under optimum conditions with high structural quality, as determined by texture analysis of the (111) pole figure, temperature dependent photoluminescence spectroscopy was conducted over the temperature range of 8.5 K to room temperature. The system and procedure for PL spectral acquisition is described in the methodology section. While optimized films demonstrate high structural quality, point defects in the system need to be characterized to determine residual doping and recombination centres that may be in the films.

A CCD detector used to capture PL spectra which reduced the time to capture data over the wavelengths of interest. However within the light collection there was an effective etalon which resulted in pronounced oscillations in the raw data. The use of CCD also limits the wavelength resolution of the measurement. Further, noise spikes appearing in the data prevented the automation of peak detection and data normalization. Power spectral analyses of the spectrum were performed in order to determine the frequency contribution of the etalon. Using this information a Butterworth low-pass filter was applied using zero-phase digital filtering. The remaining noise spikes that occurred infrequently and randomly were eliminated used a median filter with small window, less than 0.09% of the data size. A comparison of raw data to filtered data can be found in

Appendix C, demonstrating that the filter preserves both peak position and shape. The filtered data was normalized to the largest intensity peak after the noise floor of the spectrum was subtracted. In this way, relative comparisons between similar samples can be made. An approximation of the defect density relative to near edge emissions, since they appear to dominate the PL spectra, is made in this normalization as well.

Unlike high structural quality CdTe films compensated with deep level dopants, which have PL contributions from deep levels at room temperature, PL spectra at 290 K of high structural quality CdTe films grown from the undoped pressed powder targets demonstrate strong radiative transition about the expected bandgap, as seen in Figure 22.

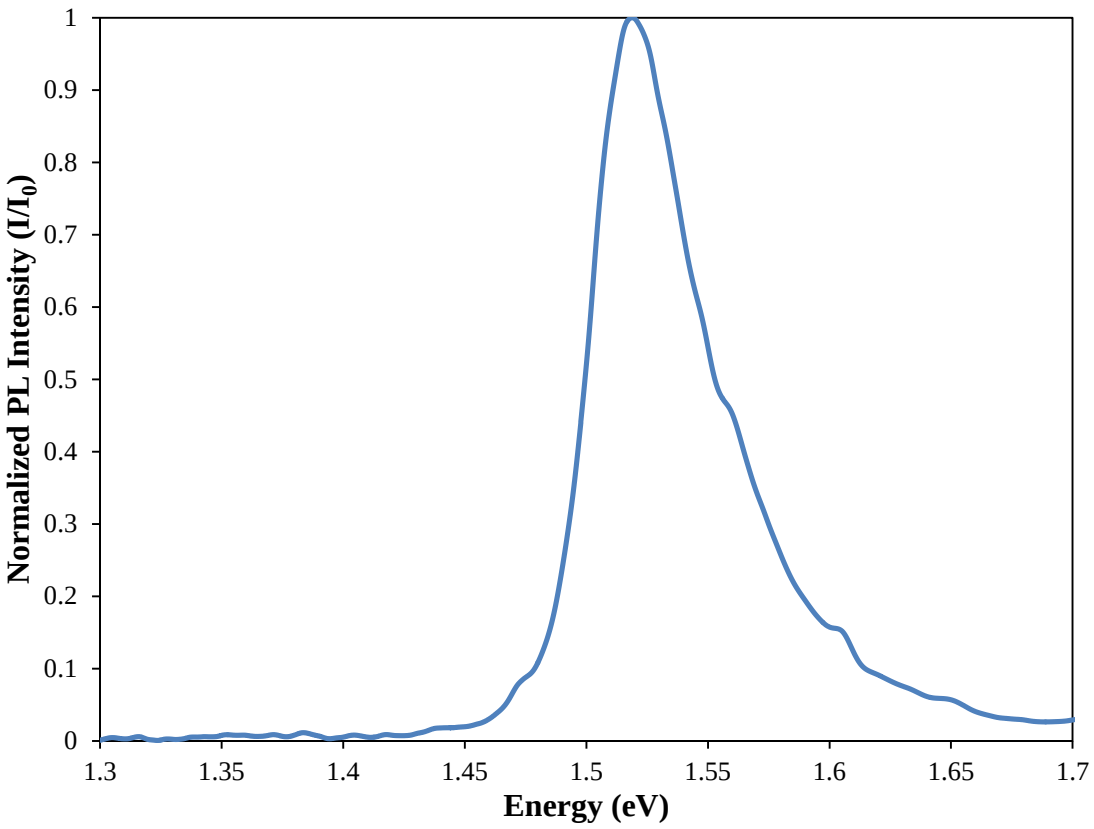

Figure 22: Normalized Intensity 290 K PL of CdTe (111)/Al_2O_3 (0001) Film Optimally Grown by PLD

Films grown at nominal thickness of 120 nm are relatively thin compared to the penetration depth of the source, a 458 nm Ar ion laser, and therefore overall PL intensity is not optimal. Radiative recombination at room temperature is expected to be band-to-band and quenched by non-radiative recombination processes. Without the presence of non-radiative recombination pathways PL spectra have strong radiative recombination band-to-band at room temperature, indicating high film quality. The bandgap of the CdTe (111)/Al_2O_3 (0001) film at 290K is ~1.53 eV; a value very close to the bulk accepted 300 K bandgap of CdTe of 1.51eV. While a slightly larger band gap for the film is expected since it is measured 10 K less than the bulk experimental expected value at 300 K, it is

also possible residual strain and inaccuracy in the measurement also account for the difference. The peak shape of the main emission resembles a Maxwell-Boltzmann distribution, seen in Equation 3, and has a narrow full width half maximum of only ~48 meV. Since band-to-band transitions should dominate the PL spectrum at room temperatures, which have Lorentzian distribution peak shapes, a Maxwell-Boltzmann line shape may be indicative of the influence of excitons in the spectrum. Gaussian smoothing of a Lorentzian could also account for this peak and be indicative of inhomogeneous strain.

For comparison the PL spectrum of a CdTe (111)/Al_2O_3 (0001) film and the CdTe (111) reference wafer are compared at a temperature of 270 K in Figure 23. Both the bulk and the film specimen had a peak emission at $E_g \approx 1.53$eV and similar line shape. The PL emission of the CdTe wafer is broader by 30 meV, which is significant since the difference is more than half of the breadth of the emission for the film.

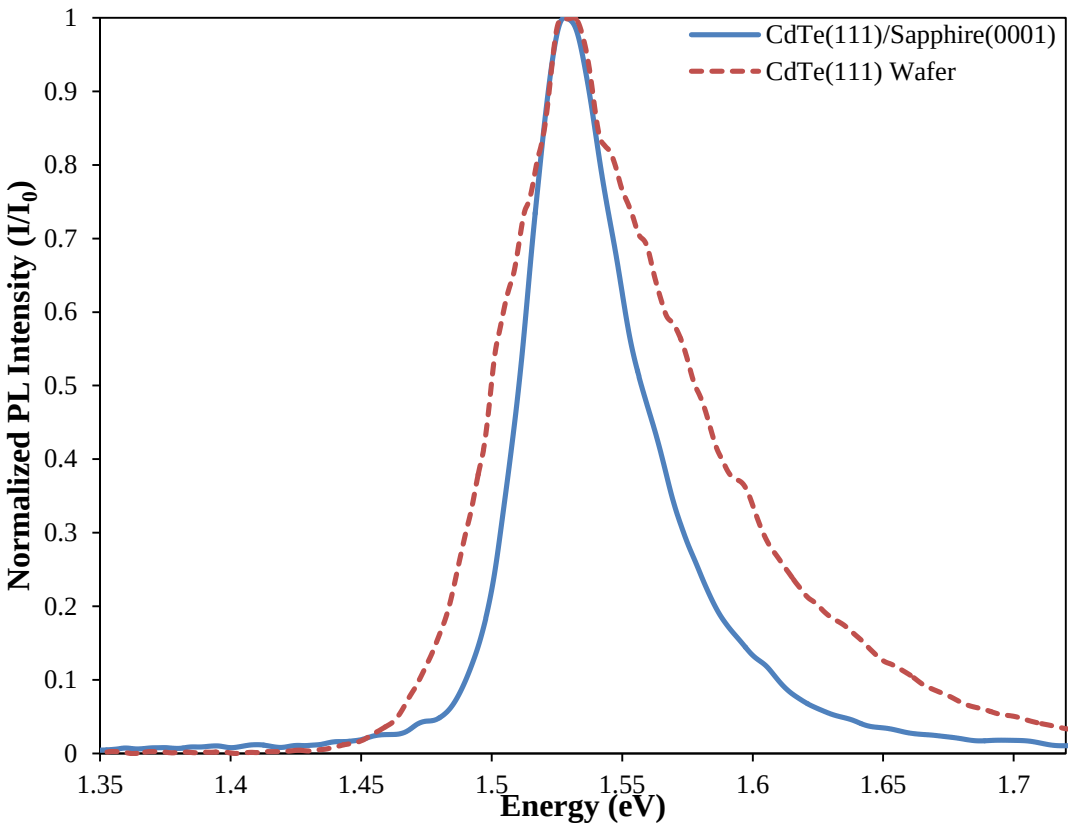

Figure 23: Normalized Intensity 270 K PL of a CdTe (111)/Al_2O_3 (0001) Film Optimally Grown by PLD and a Bulk CdTe (111) Wafer

Since direct band-to-band transitions are expected to dominate PL emission near room temperatures, it is postulated that the broadening of the wafer relative to the film is indicative of defect mechanisms causing localized band structure changes. Inhomogeneous extrinsic impurities, such as zinc, or intrinsic impurities, such as vacancies, have associated strains which cause local changes in the lattice constant and are postulated to be responsible for broadening in the wafer. The films demonstrate a more homogenous quality than the reference wafer in their smaller room temperature PL broadening parameter.

Beginning with a sample cryogenically cooled to the boiling point of liquid Helium, the PL spectrum has recombination emissions from all radiative pathways. As the temperature is raised excitons are delocalized from acceptor and donor type impurity centres and the excitons are dissociated. This transition between excitonic states and continuum transitions should occur smoothly and be continuous [80]. However, excitonic effects have been noted in the photoreflectance spectra of some III-V semiconductors up to 300K [81], which supports the Maxwell-Boltzmann line shape of PL emission for the CdTe film at 290K and 270 K indicating an intermediate regime where both emission from free excitons and direct band-to-band recombination contribute. Whereas the experimentally determined binding energy for excitons in CdTe is 10.6 meV [82], assuming excitonic contribution subtracting this binding energy from the room temperature peak PL emission the bandgap value becomes 1.52 eV; this value is much closer to the accepted bulk bandgap of 1.51 eV. The assumption of excitonic contributions at room temperature was further explored with photoreflectance.

Evaluating the PL spectrum of a sample cooled to 8.5 K, see Figure 24, high structural quality CdTe (111)/Al_2O_3 (0001) films are dominated by an excitonic emission at ~1.58 eV. The dominant peak occurs at 1.576 eV with an asymmetric shoulder on the high energy side of 1.597 eV. The spectrometer and detector used in the generation of this spectrum do not have the accuracy necessary to define specific peak positions and therefore interpretations of the associated mechanisms are educated guesses.

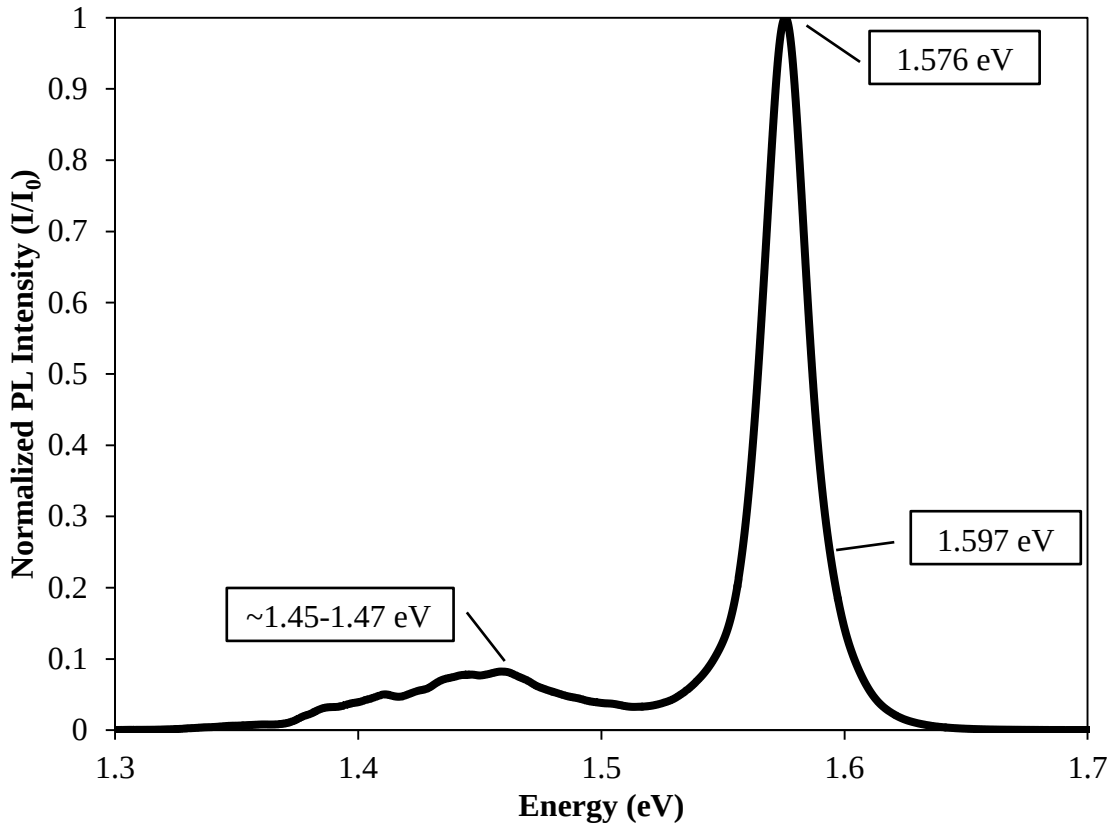

Figure 24: Normalized Intensity 8.5 K PL Spectrum of a CdTe (111)/Al_2O_3 (0001) Film Optimally Grown by PLD

Highly pure, epitaxial undoped CdTe films in literature have strong luminescence lines around 1.589 eV [83], attributed to excitons bound to residual impurities such as copper or neutral cadmium vacancy complexes. The likely candidate for the shoulder of the main PL feature, 1.597eV [84], are free excitons. In compensated material it is expected that a donor-acceptor recombination emission should occur at 1.55 eV in bulk and relaxed epitaxial CdTe [85], however, it does not occur at that position for our films. These samples had a very high resistivity as measured by the four-point probe method. PL spectroscopy results indicate the high resistivity is due to a lack of dopants rather than extrinsic or intrinsic compensation mechanisms.

Figure 24 also has a broad emission feature structured about the energy range 1.45 eV to 1.47 eV. This feature is attributed to a feature described in the literature as the 'Y-band'. The Y-band is due to the radiative recombination of excitons bound to extended defects and associated LO phonon replicas. The LO phonons replicas are separated by an energy of 21.3 meV. Such spectra have been associated with the $Te_{(g)}$ type glide dislocations in literature [86]. For comparison to our samples, high quality CdTe films grown on c-plane sapphire by molecular beam epitaxy (MBE) have a relative defect density of the Y-band of 0.07 at 77K [87]. High quality CdTe grown on c-plane sapphire by PLD had approximately the same relative defect density at 8.5 K. At 77 K it had a relative defect density for the Y-band of 0.035. This is lower than the Y-band measured for chemi-mechanically polished bulk CdTe as well [87]. While the films are not defect free, relative to MBE and even chemi-mechanically polished bulk crystal, the levels of extended defects are small indicating high crystalline and electronic quality material.

The temperature dependence of the bandgap of is most often evaluated by the Varshni equation, used commonly to describe the temperature dependence of the bandgap for IV and III-V semiconductors [88]. It has been shown that the Varshni equation is only valid when the ratio of the Debye temperature to the temperature of the sample is much less than one and a more appropriate fit is given by the Manoogian-Wooley equation below [89]:

$$E_g(T) = E_g(0K) + UT^n + V\theta\left[coth\left(\frac{\theta}{2T}\right) - 1\right] \qquad \textbf{Equation 10}$$

where the first term describes the bandgap at 0 K, the second describes the effect of thermal lattice dilation, and the last describes electron-phonon interaction. The Varshni expression lumps the effect of lattice dilation and the electron-phonon term together while Manoogian-Wooley fitting allows both to be fit to independently. If the right shoulder feature is a free exciton peak, an excitonic binding energy of ~10.6meV needs to be considered. Applying the binding energy to an empirical set of values for $E_g(T)$ from PL data as a function of temperature Figure 25 plots the empirical band gap energy as a function of temperature and a Manoogian-Wooley fit with a weighted sum of squared residuals of 0.00011085.

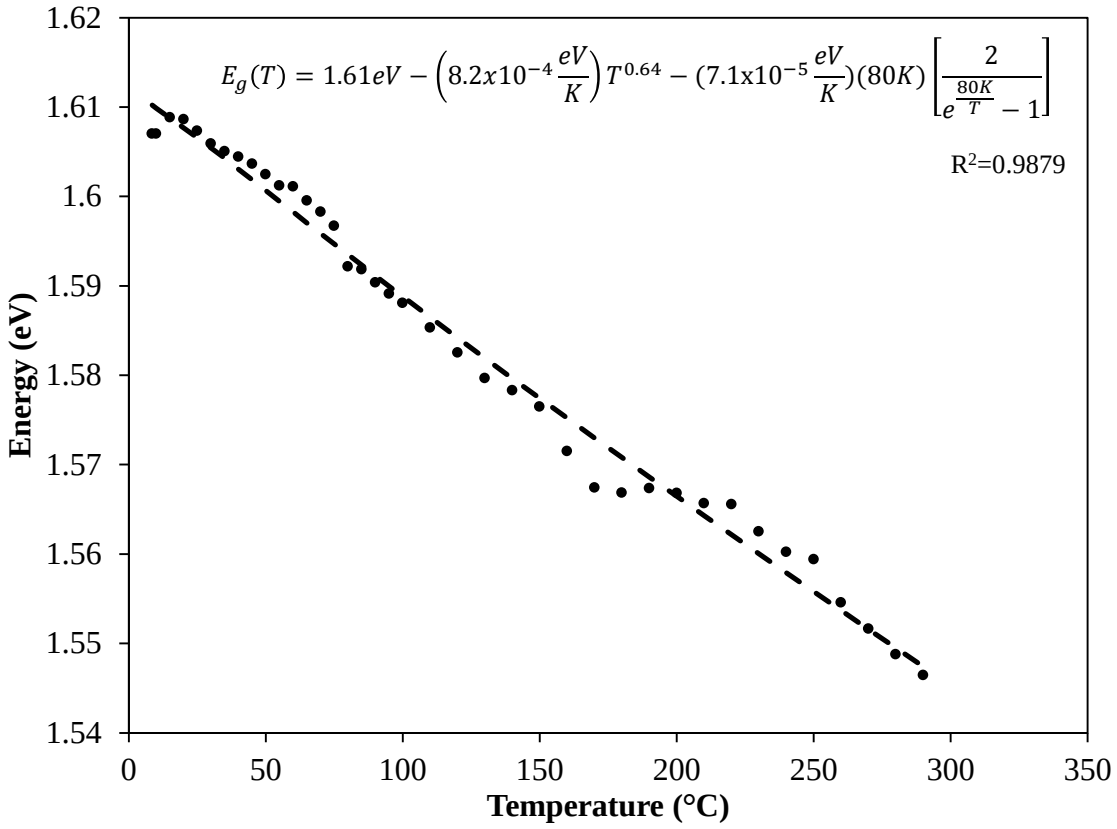

Figure 25: Manoogian-Wooley Fitting to Empirical $E_g(T)$ Derived From Temperature Dependent PL for CdTe (111)/Al_2O_3 (0001) Film Optimally Grown by PLD

The predicted 0 K bandgap agrees with the 0 K bandgap for bulk CdTe, 1.606 eV. However, the terms for the thermal dilation of the lattice and the electron-phonon interaction are lower than some reported for bulk CdTe [15]. Since the film is grown heteroepitaxially on sapphire residual strain may decrease the effect of temperature on the bandgap by constraining lattice dilation. There are a variety of scattering mechanisms for excitons in semiconductors, such as ionized impurities, piezoelectric and electron-electron scattering. A relatively low electron-phonon interaction term implies reduced

lattice phonon scattering and it is postulated that films grown under optimal conditions have high mobility.

The controlled doping of CdTe films is difficult, as discussed in chapter 1.2. CdTe polycrystalline thin films produced are often unintentionally doped with point defects such as V_{Cd}. Bulk crystal CdTe can be grown to be highly resistive or intrinsically and extrinsically doped. Efforts into in-situ doping during PLD growth led to a conductive sample, however, there was difficulty in repeating these experiments due to poor extrinsic dopants incorporation into films. Room temperature Hall effect and conductivity measurement in the Van der Pauw geometry yielded a measured resistivity of 6.25 Ω•cm, doping of 8.50×10^{14} cm^{-3} and mobility of 1189 $cm^2/V•s$ for electron carriers in the conductive single crystal CdTe film. This measurement reaffirms the high structural and optoelectronic quality of these thin films.

3.2.2 Photoreflectance and Variable Angle Spectroscopic Ellipsometry

In addition to temperature dependant PL, photoreflectance (PR) modulation spectroscopy was conducted at room temperature. The region of interest as determined from PL spectra taken at room temperature was revealed to be about an estimated bandgap of 1.5 eV. Variable angle spectroscopic ellipsometry, used originally as a characterization of sample thickness, also indicated a region of interest about 1.5 eV. Measurements of the magnitude and phase of the reflected polarization were taken at incident angles of 50° to 66° in increments of 2° for both thin CdTe (111) films and the CdTe (111) reference wafer. Fit with a Cody-Lorentz function the index of refraction, n,

and extinction coefficient, k, for both the wafer and film were determined and are summarized in Figure 26 below. The Cody-Lorentz function well describes optical resonances in semiconductors materials, whereas a Drude model well describes optical properties of metals.

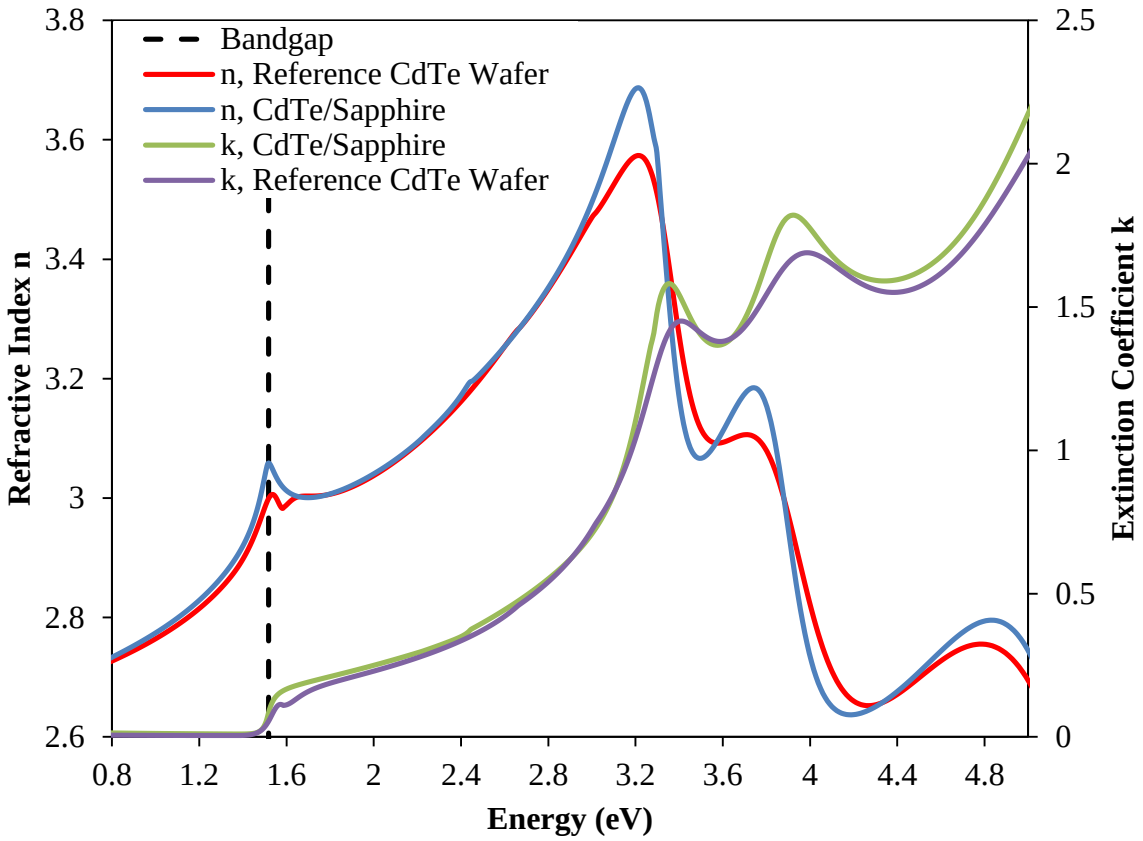

Figure 26: Variable Angle Spectroscopic Ellipsometry Cody-Lorentz Fits to Magnitude and Phase of the Reflected Polarized Light from CdTe (111) Films and a Reference CdTe (111) Wafer[1]

In order to improve the mean squared error of the model a 21.43 Å native oxide layer was included. The presence of the complex oxide was detected by atomic force microscopy and can be removed by soaking films in deionized water. This method has

[1] Ellipsometry measurement and fitting performed by Victoria Jarvis

been demonstrated for native CdTe oxide layers grown in air [90]. Under the oxide layer, the films have a root mean squared average roughness of 14.98 Å. As seen in Figure 26, the optical resonances of the film closely correspond to the reference wafer, but have sharper features. Both the n and k features around the estimated 1.5 eV bandgap, consistent with room temperature PL, for the CdTe film exceed that of the wafer, indicating a sharper optical resonance consistent with higher quality material. For energies below the bandgap, the extinction coefficient is low and nominally flat indicating little influence from free carrier absorption; consistent with the high resistivity of the films.

A low field regime was assumed for the photoreflectance analysis since there are no intentionally engineered D.C. field in these films. Further, PR spectrum are consistent with a 1.5 eV bandgap and do not indicate the presence of Franz-Keldysh oscillations. In the low field regime, theory predicts that the dielectric function should be of Lorentzian form, supported by the quality of the fit of the ellipsometric model, and so the PR spectrum should be well described by Equation 6. Fits to the room temperature PR spectra were obtained using non-linear least squares fitting. A single resonance fit described measured features well for energies $\geq E_g$. There was, however, poor agreement with the spectrum below the bandgap. Due to the Maxwell-Boltzmann line shapes seen in room temperature PL spectra, it was postulated that a second resonance at room temperature in the measured spectrum was the cause. A double resonance fit, the superposition of two optical resonances in Figure 27 describes both excitonic and continuum band-to-band radiative transitions. Excitonic contributions in room

temperature PR spectra have been investigated in literature for high quality CdTe material [91], [92].

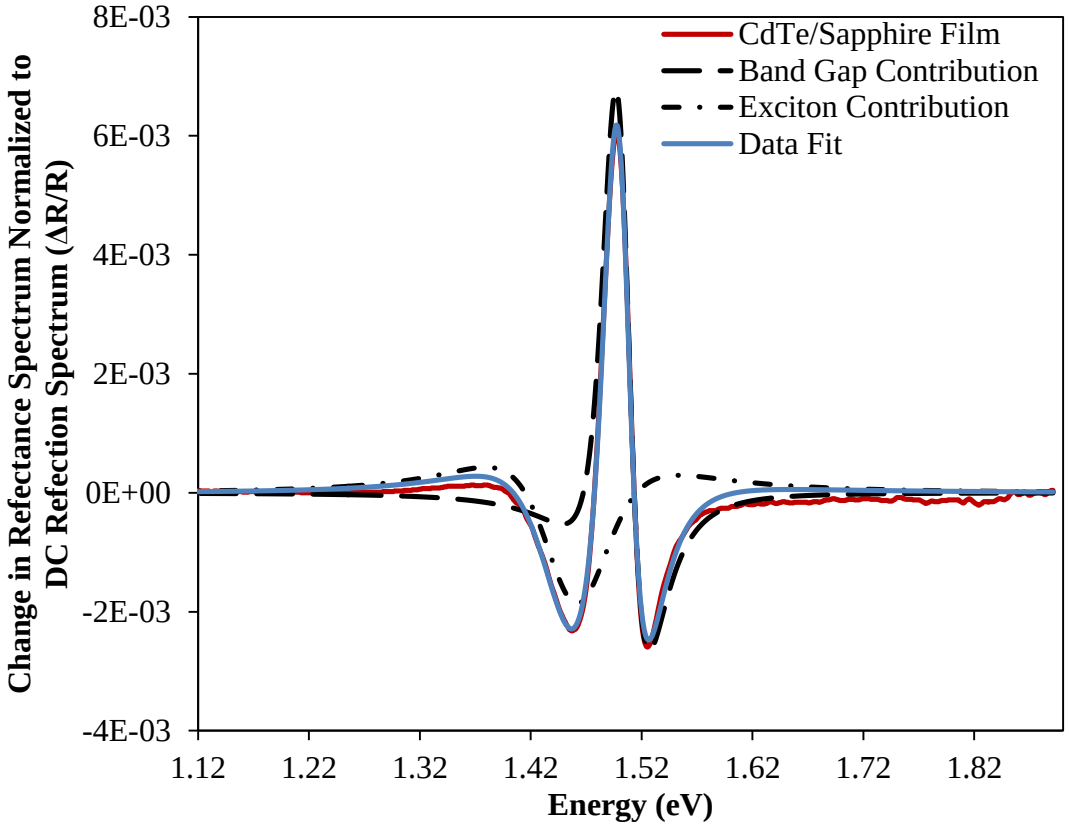

Figure 27: Room Temperature PR Spectra of CdTe (111)/Al_2O_3 (0001) Film Optimally Grown by PLD with Two Resonance Fitting

In the fitting parameters used for the direct radiative contribution the value of m was constrained to be 2.5 [67], as suggested in literature for materials with a direct gap at the three dimensional critical point. As previously discussed, the recursive form of the Gaussian is numerically estimated by applying Equation 6 and allowing the value of m to be a variable in the fitting. The double resonance fit to the PR spectrum in Figure 27 reduces the mean square error to 1.1E-5 and improves the R^2 value to 0.98 from a single

resonance fit. The band-to-band optical resonance is fit with the parameters: E_g=1.51 eV, Γ_1=39 meV, Φ_1=6.7 Rad, C_1=5.4E-6 and m_1=2.5. The excitonic optical resonance is fit with the parameters: E_e=1.50 eV, Γ_2=52 meV, Φ_2=4.2 Rad, C_2=2.4E-6 and m_2=3. The difference between the fitted radiative band-to-band and excitonic optical resonance contribution yield a binding energy of 10 meV for the exciton. This value relative to the discussed 10.6 meV value from literature demonstrates strong agreement.

The broadening parameter for the band-to-band contribution, Γ_1, is small and well within the range of experimentally observed broadening parameters for high quality materials [93]. The broadening parameter is expected to increase proportionally to the sample defect density due to scattering and trapping effects at point defect and defect complexes. A decrease in crystallographic quality can also increase the broadening parameter as scattering and trapping effects can occur at grains, threading dislocations, anti-phase boundaries and twin collisions. The two multiplication constants C_1 and C_2 yield no independent information about the sample since they are measurement system dependent. The difference between them indicates that direct radiative contributions are greater than excitonic contributions. This was expected since the contribution of the radiative recombination of excitons should decrease with increasing temperature. Similarly, while the phase values Φ_1 and Φ_2 of the optical contributions does not reveal any unique information about the sample, they are internally consistent in that the timescale for direct radiative recombination is less than excitonic radiative recombination and therefore Φ_1 is greater than Φ_2.

Comparison of the obtained PR spectrum to other near band edge photoreflectance spectrum and fitting for high quality CdTe materials reveal both similar trends and values. Particularly a fitted critical point value of m_2=3 [91] for the Gaussian excitonic approximation is noted in literature [65]. The obtained PR spectrum and fitting parameters are consistent with undoped high quality CdTe. The electro-optic features of the measured PR spectrum, such as a 1.51 eV bandgap, room temperature exciton presence and low defect density, are consistent with ellipsometric and PL measurements. Sample spectra collected by the various optical techniques homogeneously demonstrate that the high resistance of the CdTe films is due to the lack of charge carriers rather than the presence of trap and scattering mechanisms.

3.3 Freestanding CdTe Thin Films

Concurrent with the growth optimization of CdTe (111) films on Al_2O_3 (0001), MgO (111) and the native oxide of Si (100) substrates yielded an unexpected and significant result. In order to measure the electrical properties of undoped films metal contacts were lithographically applied; doping attempts of films were made in-situ and post growth as well. The subsequent lift-off to form contacts in the Van der Pauw geometry on the films resulted in the detachment of the CdTe film from sapphire. The film remained bonded to the metal film and intact. In subsequent experimentation, peeling and pulling crystalline CdTe films off of sapphire using various tapes, glues, epoxies, photoresists and polymer secondary carriers revealed that the degree of twinning in original film did not play a significant role in its detachment. Instead the dominant factor in the yield of film from the

substrate during a peel or pull was proportional to strength of the bond between the film and secondary carrier as well as the film thickness. Stringent preparation of the secondary carrier, by solvent cleaning, and epitaxial film, deionized water soak, prior lift-off attempt proved necessary to improve yield consistency.

Single crystal films, 12 mm by 12 mm in size, were able to be removed by epoxy bonding, solder reflow bonding and polymer carrier techniques with and without the assistance of cryogenic dipping in LN_2. While films bonded strongly to a secondary carrier could be manually pulled from the sapphire, the application additional force from sources such as sonication, heating and cooling cause the film to detach without the need for manual peeling. Detached films left their substrate undamaged and suitable for repeated heteroepitaxial growth. Study into this ‘regrowth’ revealed that samples grown on substrates which had films detached from them under the same growth parameters had crystal structures as determined by generated (111) pole figures, as seen in Figure 28 below.

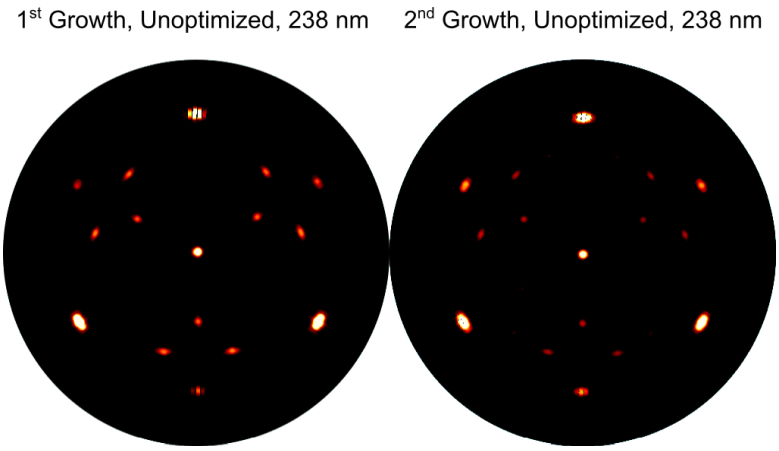

Figure 28: 2DXRD Stereographic (111) Projections of a CdTe (111) Thin Film Repeated Growth on Identical Substrates Following Detachment, Identical Growth Conditions with Different Growth Times

Both samples in Figure 28 were grown before the single crystal growth of CdTe was optimized for the undoped pressed powder target. As well, the second growth displayed above on the left, while under the same growth conditions, was grown for less time. Therefore, the regrown sample thickness was less than the first growth. It is postulated that the 2nd order twinning, a symmetric rotation about the host out of the growth plane, seen as the inner nine peaks were growth twin and therefore had less intensity in the thinner sample. Regardless, since the host lattice and degree of twinning is equivalent between the growths, the substrate following a film detachment was provided the same heteroepitaxial template for the secondary growth. After repeated regrowth process it appears that the c-plane sapphire substrate can be used as an indefinite epitaxial template for CdTe thin film growth. This is unlike other thin film detachment techniques such as chemically etching sacrificial layers or ion implantation and exfoliation where substrate reuse is finite.

In addition to the reusability of the sapphire substrate and the consistency in templating new epitaxial CdTe films, films removed from their substrate onto rigid and flexible carriers were structurally analysed using 2DXRD. Initial testing with polymer and epoxy carriers led to cracking of the films. Cracking occurred preferentially, with relation to the substrate orientation and was believed to be a cleaving process. Epoxy bonding of films to rigid carriers such as glass, silicon and sapphire drastically improved the yield of pristine film from the substrate and provided a mechanism of leverage for peeling the films. Whole films were released onto sapphire substrates and analysed structurally with 2DXRD texture analysis. The film epitaxially aligned on the c-plane sapphire substrate and epoxied to sapphire carrier, seen in Figure 28, revealed no change in crystal structure from the release process.

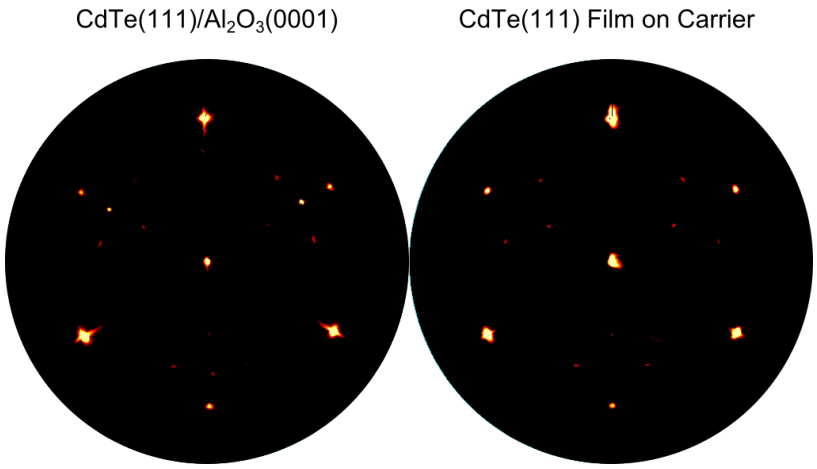

Figure 29: 2DXRD Stereographic (111) Projections of a CdTe (111) Thin Film Before and After Lift-off (111)

As seen previously for non-optimally as-deposited CdTe the pole figures indicate a majority phase of CdTe epitaxially aligned with the sapphire substrate with a minority of

twin phases. The pole figures after the release of the film indicated no change in crystalline quality, since they contain no additional x-ray reflections and the peak broadness did not chance. The included central peak in the above pole figures illustrated that both films had their layers stacked in parallel to the substrate and carrier respectively. Further, it demonstrates the breadth and intensity of all peaks are equivalent. The decrease in radial broadening after lift-off is consistent with elastic strain relaxation.

The flatness of released films, as measured seen in scanning electron micrographs and measured by atomic force microscopy, revealed that the films remained atomically smooth. As such, an equivalent intensity, broadness and shape for all the peaks after the release of the film indicated that both the nominal flatness and crystallinity of the film is maintained when released. Generated pole figures support that while the sample was epitaxially aligned to the sapphire after growth, when epoxied to a sapphire carrier and released from the growth substrate the epitaxial relationship is lost. At this point the film was classified as ‘free-standing’ on a secondary carrier. 2DXRD analysis conducted on further epitaxial growth on the released CdTe film would reveal applications of the technology as buffer layers. This is likely since they are structurally identical to the as-deposited films.

CdTe films as-deposited and after release were also characterized by low temperature photoluminescence spectroscopy. The films maintained optoelectronic quality, as seen in Figure 30, in addition to their structure. In the case of the as-deposited film the photoluminescence spectrum at 10K has an attributed majority contributions from

attributed edge emission at 1.54 eV, a shoulder excitonic contribution at 1.56 eV and a small shoulder contribution from a free excitonic peak at 1.60 eV. Recall that for optimally grown CdTe (111) films grown on c-plane sapphire, the dominant features PL spectrum features at 10K were attributed to a bound exciton emission about 1.57 eV and a shoulder emission about 1.60 eV. Direct comparison of the PL spectrum between samples is difficult because of difference in thickness, and growth parameters. As well, the differences from collected spectra from one side polish and two side polish substrates are not accounted for between the released film investigation and the original low temperature PL for quality optimization investigation respectively. Since the two measurements in Figure 30 are of the same film, as-deposited and released, and the carrier is identical to the substrate the only difference to be considered between the spectrums was be the influence of the release process and the influence of epoxy bonding of the film to the carrier. Both the decrease in broadening and right shifting of the peak after lift-off is consistent with strain relaxation observed in 2DXRD.

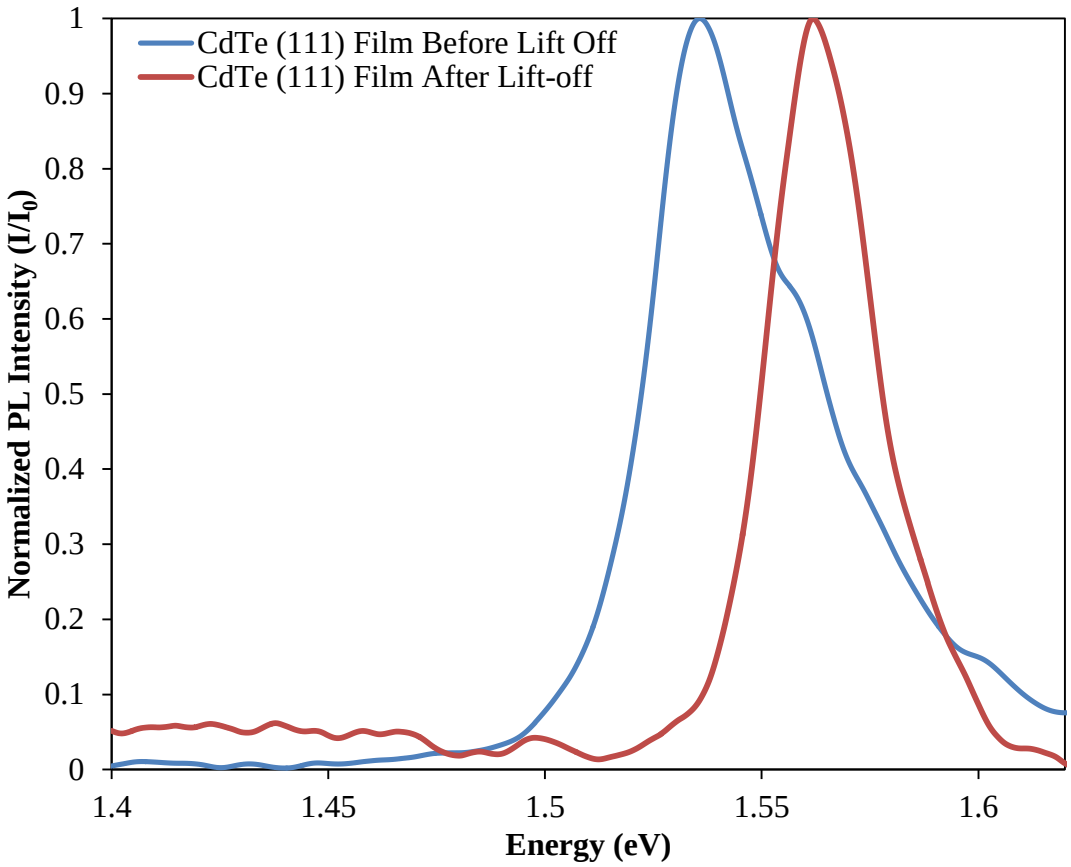

Figure 30: Normalized 10K PL Spectrum of CdTe (111) Film (Left) Before and (Right) After Lift-off

The released films had a narrow PL spectrum with an attributed bound excitonic emission about 1.56 eV and a free excitonic shoulder about 1.60 eV. Both films had strong low temperature PL and excitonic contributions. The released film indicates a higher excitonic contribution to its low temperature PL spectrum than the as-deposited film. It is postulated that the mechanism of release is an interfacial defect which accommodates strain after a critical thickness. This is consistent with the postulation made, recalling Figure 20, that there is a defect network at the interface. In order to

further study the mechanism of release high resolution transmission electron microscopy of both the CdTe/sapphire interface and free standing CdTe films are required.

Despite epitaxial alignment to the c-plane sapphire substrate, the ease of release of the CdTe film in combination with the maintenance of its structural and optoelectronic properties suggest that the basic separation energy for bonds across the interface, the work of adhesion, is lowered or compensated prior lift-off attempts. A driving force for film release could be the uniform tensile stress from the epitaxial mismatch between CdTe and the sapphire. Decohesion of thin metal films, under tensile stress from epitaxy, on ceramic substrates has been empirically studied [94] and theoretically modelled [95], [96]. It is hypothesized that a defect network at the interface accommodates heteroepitaxial strain by plastic deformation and film release from the substrate. The multi-valency of tellurium may also play a role in the stabilization of the interface after plastic reconstruction. The combination of density functional theory modelling, transmission electron microscopy and study of the interface debond energy will play a large role in understanding the mechanism of film release. Conversely, bonding experiments to form structures with thin films will capitalize on technological value. At the time of writing this thesis, this discovery is covered under the United States provision patent application number 61/683317, *Arbitrarily Thin Ultra Smooth Film with Built-in Separation Ability and Method of Forming the Same*.

Chapter 4 - Conclusions

Using 2DXRD texture analysis techniques for structural characterization the growth of undoped CdTe (111)/Al_2O_3 (0001) from the PLD of a pressed powder target has been optimized to yield single crystal films. The growth of these high quality films occurs at energy densities ~2 J/cm^2, a laser repetition rate of 0.5 Hz and a substrate temperature of 300°C; a temperature of 320°C is required for one side polished c-plane sapphire substrates. A laser fluence of 2 J/cm^2 is obtained for a 90 mJ stabilized energy beam with reduced dimensions of 15 mm by 6.3 mm beam, focused to an image size of 4.5 mm^2. The 12 mm by 12 mm substrate is uniformly coated by the plume at a target-substrate separation of 8 cm. The net deposition rate at the optimum growth temperature is 0.33 Å/pulse. The penetration depth of the excimer laser into the target is approximated to be 1 nm assuming conservation of mass of the plume to the film. Increasing the target substrate distance further should allow for higher later repetition rates and faster net growth rates.

While uniformity in temperature profile across the furnace is an issue, the growth temperature, as measured by a thermocouple at the radial edge of the furnace, has little temperature dependence on the thickness of the film. This is postulated to be because of the increased stability in CdTe bonds relative to their constituents bonding strengths and strong drive to maintain 50:50 stoichiometry at the growth temperature. The temperature dependence on the film quality, as characterized by the ratio of the first order twin peak

intensity in the (111) pole figure relative to the host lattice peak, indicated that film quality was improved with increasing temperature until sublimation from the film became non-negligible relative to the growth rate. Similarly, the film thickness was inversely squared proportional to the structural quality of the film, hypothesised to be due to a stacking fault or equivalent defect localized at the interface where a strain relaxation occurs.

Comparing the (111) pole figure for optimally grown single crystal CdTe (111) films and a reference CdTe (111) wafer illustrated that they are of equivalent structural quality. Overlaying the normalized PL spectrum at 270 K of a high quality film and the reference wafer demonstrated agreement in peak emission location and that film emission about that peak has a smaller broadening parameter. Low temperature normalized PL spectroscopy of CdTe films indicated a dominant peak emission at 1.58 eV with a shoulder emission at 1.60 eV. These are attributed to a bound exciton emission and a free exciton emission respectively. Y-band emission, attributed to Te glide dislocations at the substrate interface, were shown to be 2 times smaller in quality high CdTe films grown on sapphire by PLD than those grown in literature by MBE. The pronunciation of the Y-band in low temperature PL spectra is postulated to be film thickness dependant.

The temperature dependence of the bandgap, as determined from peak fitting to PL spectra, was well fit by the Manoogian-Wooley model. The temperature dependence, related to lattice dilation, of single crystal films heteroepitaxially grown on sapphire was less than for bulk single crystals reported in literature. This is conjectured to be due to un-

relaxed strain, since the temperature dependant lattice dilation of sapphire is one order smaller than for CdTe. Regardless, both data from temperature dependant PL spectra and 2DXRD are consistent with high quality, undoped material. High room temperature mobility reported for low n-type doping in films is congruous with the hypothesis that the high resistance of undoped films is the result of the material's wide bandgap and lack of carriers rather than high defect densities.

Observations of high quality films and a reference wafer by variable angle spectroscopic ellipsometry are consistent with PL spectroscopic observations at the room temperature. Overlapping optical resonance positions in ellipsometry indicate that radiative emissions are of the same energy for the film and wafer. However, optical resonances were sharper for the films suggesting higher material quality. Ellipsometry predicted a thin native oxide on the films and wafer detected by atomic force microscopy. PR spectra obtained at room temperature were fit in the low field regime. The bandgap of the films at room temperature was found to be 1.51 eV, agreeing with measurements of the bandgap taken by ellipsometry, PL spectroscopy and literature. A narrow direct radiative transition broadening parameter and the presence of excitons was fit to the PR spectrum coherently reinforcing the observed Maxwell-Boltzmann line shapes in PL spectrum and the high quality of the films.

Parallel to the optimization of the films it was demonstrated that the films could be released from oxide substrates onto a carrier substrate, maintaining their structural and optoelectronic quality. Further, the substrate could be used to epitaxially grow subsequent

films and perform releases, seemingly indefinitely. It is speculated that the mechanism of release is a defect network at the interface which through plastic relaxation accommodates heteroepitaxial strain. In addition, decoherence of the film spontaneously from the substrate when heated, cooled or sonicated implies the number of bonds and/or energy of breaking those bonds must be small relative to the combination of heteroepitaxial and thermal strain. The technology was provisionally patented as it is applicable for the development cost benefit of technologies such as radiation detectors, infrared detectors and photovoltaics. At the time of writing this thesis, work regarding the release of the CdTe films from sapphire substrates is covered under United States provision patent application number 61/683317, *Arbitrarily Thin Ultra Smooth Film with Built-in Separation Ability and Method of Forming the Same*. While high quality CdTe buffer layers and devices released from sapphire offer a platform for various technologically relevant devices and structures, further study into the mechanism of release may reveal how the technology can be applied to other material systems.

Chapter 5 - Future Work

5.1 Doping Study

Optimally grown single crystal CdTe (111) films grown on c-plane sapphire are undoped and non-conducting, limiting their practical usefulness as and in semiconducting devices. From a device and engineering standpoint the practicality of semiconductors come from the ability to precisely defect engineer them intrinsically or extrinsically to

modify the resistivity and majority charge carrier population. In order to create simple devices with this high quality material a doping study should be conducted. Post growth annealing with a controlled overpressure of Cd and Te has been shown in literature to modify the Fermi energy of CdTe single crystals [97]. As well, in-situ doping using doped CdTe targets, alternating pulses between CdTe and a dopant target or adding a doping plasma source, such as nitrogen, to the growth chamber should be considered. Ion implantation and thermal activation may also be an option. For contact and shallow junction doping, preliminary excimer laser doping tests, based upon recipes for doping single CdTe bulk crystals in literature, were promising [24].

5.2 Wafer Bonding

Detaching the CdTe film from c-plane sapphire substrates allows for the direct study of the interface in order to determine the mechanism of release. Such an interface would normally be buried. However, the real commercial benefit from this discovery comes from the integration of high quality films and structures with low cost and readily available substrates such as silicon, glass and plastic. High quality thin films and structures can be used as the key component in a variety of microelectronic, optoelectronic, photovoltaic and imaging devices. As such, studying the bonding of single crystal CdTe onto carriers is crucial to the development of the technology. Focusing first on bonding CdTe films using techniques such as oxide and adhesive bonding will help produce single crystal CdTe buffer layers. A single crystal thin film on a structurally and thermally stable secondary carrier supplements the need for CdTe wafer epitaxial growth.

Secondly, wafer bonding CdTe films using diffusion or eutectic bonding techniques to standard readout integrated circuits and doped wafers allow for the production of electrically and optically integrated film-wafer structures. The combination of these two techniques and the reuse of the sapphire substrate constitute the basis for all devices produced utilizing this technology.

References

[1] *Joint Committee for Powder Diffraction Standards Card Number 15-770,* 1972.

[2] *Joint Committee for Powder Diffraction Standards Card Number 19-193,* 1998.

[3] S. Wei and S. B. Zhang, "Structure Stability and Carrier Localization in CdX(X=S, Se, Te) Semiconductors," *Physical Review B,* vol. 62, no. 11, pp. 6944-6947, 2000.

[4] S. M. Hosseini, "Optical Properties of Cadmium Telluride in Zinc-blende and Wurzite Structure," *Physica B: Condensed Matter,* vol. 403, no. 10-11, pp. 1907-1915, 2008.

[5] S. Neretina, Q. Zhang, R. A. Hughes, J. F. Britten, N. V. Sochinskii, J. S. Preston and P. Mascher, "The Role of Lattice Mismatch in the Deposition of CdTe Thin Films," *Journal of Electronic Materials,* vol. 35, no. 6, pp. 1224-1230, 2006.

[6] S. Neretina, R. A. Hughes, J. F. Britten, N. V. Sochinskii, J. S. Preston and P. Mascher, "Vertically Aligned Wurtzite CdTe Nanowires Derived from a Catalytically Driven Growth Mode," *Nanotechnology,* vol. 18, no. 27, 2007.

[7] Y. Yan, M. M. Al-Jassim, K. M. Jones, S. Wei and S. B. Zhang, "Observation and First-principles Calculation of Buried Wurtzite Phases in Zinc-blende CdTe Thin Films," vol. 77, no. 10, pp. 1461-1463, 2000.

[8] D. W. Niles and H. Höchst, "Critical Test of CdTe (100) Angle-resolved Photoemission Spectra with Band-structure Calculations," *Physical Review B,* vol. 43, no. 2, pp. 1492-1499, 1991.

[9] J. R. Chelikowsky and M. L. Cohen, "Nonlocal Pseudopotential Calculations for the Electronic Structure of Eleven Diamond and Zinc-blende Semiconductors," *Physical Review B,* vol. 14, no. 2, pp. 556-582, 1976.

[10] K. Pastor, "Influence of the Electron-electron Interaction on the Cyclotron Resonance Half-width in Bulk CdTe," *Physical Review B,* vol. 37, no. 15, pp. 8895-8898, 1988.

[11] R. Triboulet and P. Siffert, CdTe and Related Compounds; Physics, Defects, Hetero- and Nano-structures, Crystal Growth, Surfaces and Applications, Amsterdam: Elsevier Science, 2009.

[12] V. Vyas and B. K. Sharma, "Study of Bonding ZnSe and CdTe by Compton Scattering Technique," *Chalcogenide Letters,* vol. 7, no. 5, pp. 335-337, 2010.

[13] K. Zanio, "Volume 13: Cadmium Telluride," in *Semiconductors and Semimetals*, New York, Academic Press, 1978.

[14] T. E. Schlesinger, J. E. Toney, H. Yoon, E. Y. Lee, B. A. Brunett, L. Franks and R. B. James, "Cadmium Zinc Telluride and its Use as a Nuclear Radiation Detector Material," *Material Science and Engineering Reports*, vol. 32, no. 4-5, pp. 103-189, 2001.

[15] G. Fonthal, L. Tirado-Mejía, J. I. Marín-Hurtado, H. Ariza-Calderón and J. G. Mendoza-Alvarez, "Temperature Dependence of the Band Gap Energy of Crystalline CdTe," *Journal of Physics and Chemistry of Solids*, vol. 61, no. 4, pp. 579-583, 2000.

[16] B. Segall, "Optical Absorption Edge in CdTe: Theoretical," *Physical Review*, vol. 150, no. 2, pp. 734-747, 1966.

[17] D. T. Marple, "Effective Electron Mass in CdTe," *Physical Review*, vol. 129, no. 6, pp. 2466-2470, 1963.

[18] A. L. Mears and R. A. Stradling, "Cyclotron Resonance and Cross-modulation with n-type CdTe at 1 mm and 2 mm Wavelength," *Solid State Communications*, vol. 7, no. 17, p. 1267–1269, 1969.

[19] L. S. Dang, G. Neu and R. Romestain, "Optical Detection of Cyclotron Resonance of Electron and Holes in CdTe," *Solid State Communications*, vol. 44, no. 8, pp. 1187-1190, 1982.

[20] S. Wei and S. B. Zhang, "Theoretical Study of Doping Limits of CdTe: Preprint," in *NCPV Program Review Meeting*, Lakewood, 2001.

[21] G. Mandel, "Self-Compensation Limited Conductivity in Binary Semiconductors. I. Theory," *Physical Review*, vol. 134, no. 4A, pp. A1073-A1079, 1964.

[22] F. Fischer, A. Waag, G. Bilger, T. Litz, S. Scholl, M. Schmitt and G. Landwehr, "Molecular Beam Epitaxy of Iodine-doped CdTe and (CdMg) Te," *Journal of Crystal Growth*, vol. 141, no. 1-2, pp. 93-97, 1994.

[23] R. B. Hall and H. H. Woodbury, "The Diffusion and Solubility of Phosphorus in CdTe and CdSe," *Journal of Applied Physics*, vol. 39, no. 12, pp. 5361-5365, 1968.

[24] Y. Hatanaka, M. Niraula and T. Aoki, "Excimer Laser Doping Techniques for II–VI Semiconductors," *Applied Surface Science*, Vols. 175-176, pp. 462-467, 2001.

[25] S. G. Meikle and D. A. Thompson, "Rapid Thermal Annealing of Ion Implanted CdTe," *Journal of Electronic Materials*, vol. 16, no. 3, pp. 157-161, 1987.

[26] A. Zunger, "Practical Doping Principles," *Applied Physics Letters*, vol. 83, no. 1, pp. 57-59, 2003.

[27] M. N. Abedin, T. F. Refaat, J. M. Zawodny, S. P. Sandford, U. N. Singh, S. V. Bandara, S. D. Gunapala, I. Bhat and N. P. Barnes, "Multicolor Focal Plane Array Detector Technology: a Review,"

in *SPIE 5152, Infrared Spaceborne Romote Sensing XI*, San Diego, 2003.

[28] C. Yuanping, "Molecular Beam Epitaxial Growth of High-Quality Cadmium Telluride on Silicon," University of Illinois at Chicago, Chicago, 1995.

[29] A. Rogalski, "Recent Progress in Infrared Detector Technologies," *Infrared Physics & Technology,* vol. 54, no. 3, pp. 136-154, 2011.

[30] Y. Xin, N. D. Browning, S. Rujirawat, S. Sivananthan, Y. P. Chen, P. D. Nellist and S. J. Pennycook, "Investigation of the Evolution of Single Domain (111)B CdTe Films by Molecular Beam Epitaxy on Miscut (001)Si Substrate," *Journal of Applied Physics,* vol. 84, no. 8, pp. 4292-4299, 1998.

[31] Y. Chen, S. Farrell, G. Brill, P. Wijewarnasuriya and N. Dhar, "Dislocation Reduction in CdTe/Si by Molecular Beam Epitaxy Through In-situ Annealing," *Journal of Crystal Growth,* vol. 310, no. 24, pp. 5303-5307, 2008.

[32] J. M. Arias, J. G. Pasko, M. Zandian, S. H. Shin, G. M. Williams, L. O. Bubulac, R. E. DeWames and W. E. Tennant, "Planar p-on-n HgCdTe Heterostructure Photovoltaic Detectors," *Applied Physics Letters,* vol. 62, no. 9, pp. 976-978, 1993.

[33] International Atomic Energy Agency, "Nucleus: For Nuclear Knowledge and Information - NuDat 2," 2012.

[34] C. Szeles, "CdZnTe and CdTe Materials for X-ray and Gamma Ray Radiation Detector Applications," *Physica Status Solidi (b),* vol. 241, no. 3, pp. 783-790, 2004.

[35] M. J. Yaffe and J. A. Rowlands, "X-ray Detectors for Digital Radiography," *Physics in Medicine and Biology,* vol. 42, no. 1, 1997.

[36] Y. Eisen and A. Shor, "CdTe and CdZnTe Materials for Room-temperature X-ray and Gamma Ray Detectors," *Journal of Crystal Growth,* Vols. 184-185, pp. 1302-1312, 1998.

[37] A. Fauler, J. Konrath, V. Babentsov, J. Franc and R. B. James, "Comparison of Undoped and Doped High Resistivity CdTe and (Cd,Zn)Te Detector Crystals," *IEEE Transactions on Nuclear Science,* vol. 51, no. 4, pp. 1864-1868, 2004.

[38] M. Osborne, "NREL Confirms Latest CdTe Module Efficiency Record from First Solar," Solar Media Limited, 17 January 2012. [Online]. Available: http://www.pv-tech.org/news/nrel_confirms_latest_cdte_module_efficiency_record_from_first_solar.

[39] M. Osborne, "First Solar to Speed-up Implantation of CdTe Cell Efficiency Gains," Solar Media Limited, 19 June 2012. [Online]. Available: http://www.pv-tech.org/news/first_solar_to_speed_up_implantation_of_cdte_cell_efficiency_gains.

[40] A. Morales-Acevedo, "Can we Improve the Record Efficiency of CdS/CdTe Solar Cells?," *Solar*

Energy Materials and Solar Cells, vol. 90, no. 15, pp. 2213-2220, 2006.

[41] M. Peters, J. C. Goldschmidt and B. Bläsi, "Angular Confinement and Concentration in Photovoltaic Converters," *Solar Energy Materials and Solar Cells,* vol. 94, no. 8, pp. 1393-1398, 2010.

[42] R. Brendel and H. J. Queisser, "On the Thickness Dependence of Open Circuit Voltage of p-n Junction Solar Cells," *Solar Energy Materials and Solar Cells,* vol. 29, no. 4, pp. 397-401, 1993.

[43] M. Burgelman, J. Vershraegen, S. Degrave and P. Nollet, "Analysis of CdTe Solar Cells in Relation to Material Issues," *Thin Solid Films,* Vols. 480-481, pp. 392-398, 2005.

[44] S. Neretina, R. A. Hughes, J. F. Britten, N. V. Sochinskii, J. S. Preston and P. Mascher, "The Role of Substrate Surface Termination in the Deposition of (111) CdTe on (0001) Sapphire," *Applied Physics A,* vol. 96, no. 2, pp. 429-433, 2009.

[45] P. D. Tepesch and A. A. Quong, "First-Principles Calculations of α-Alumina (0001) Surfaces Energies with and without Hydrogen," *Physica Status Solidi (b),* vol. 217, no. 1, pp. 377-387, 2000.

[46] C. Scharager, P. Siefert, P. Höschl, P. Moravec and M. Vaněček, "Characterization of Germanium-doped CdTe Crystals," *Physica Status Solidi (a),* vol. 66, no. 1, pp. 87-92, 1981.

[47] R. K. Singh and J. Narayan, "Pulsed-laser Evaporation Technique for Deposition of Thin Films: Physics and Theoretical Model," *Physical Review B,* vol. 41, no. 13, pp. 8843-8859, 1990.

[48] L. A. Golovan, B. A. Markov, P. K. Kashkarov and V. Y. Timoshenko, "Evaporation Effect on Laser Induced Solid–liquid Phase Transitions in CdTe and HgCdTe," *Solid State Communications,* vol. 108, no. 10, pp. 707-712, 1998.

[49] E. Robert, Pulsed Laser Deposition of Thin Films: Applications-Led Growth of Functional Materials, Hoboken: John Wiley & Sons, 2007.

[50] R. Diamant, L. Ponce, M. Fernández and E. Jiménez, "Plasma Dynamics and its Relationship with Thin Film Properties of CdTe via Pulsed Laser Deposition (PLD)," *Applied Physics B,* vol. 66, no. 5, pp. 639-643, 1998.

[51] J. M. Warrender and M. J. Aziz, "Morphological Evolution of Ag/Mica Films Grown by Pulsed Laser Deposition," in *MRS Proceedings*, 2002.

[52] D. B. Chrisey and G. K. Hubler, Pulsed Laser Deposition of Thin Films, Wiley-VCH, 2003.

[53] C. C. Chang, "LEED Studies of the (0001) Face of α-Alumina," *Journal of Applied Physics,* vol. 39, no. 12, pp. 5570-5573, 1968.

[54] F. Cuccureddu, S. Murphy, I. V. Shvets, M. Porcu, H. W. Zandbergen, N. S. Sidorov and S. I. Bozhko, "Surface Morphology of c-plane Sapphire (α-Alumina) Produced by High Temperature Anneal,"

Surface Science, vol. 604, no. 15-16, pp. 1294-1299, 2010.

[55] V. V. Godlevsky, J. J. Derby and J. R. Chelikowsky, "Ab Initio Molecular Dynamics Simulation of Liquid CdTe and GaAs: Semiconducting versus Metallic Behavior," *Physical Review Letters,* vol. 81, no. 22, pp. 4959-4962, 1998.

[56] E. E. Guzzo and J. S. Preston, "Laser Ablation as a Processing Technique for Metallic and Polymer Layered Structures," *IEEE Transactions on Semiconductor Manufacturing,* vol. 7, no. 1, pp. 73-78, 1994.

[57] T. Aoki, O. S. Gorodnychenko and Y. Hatanaka, "Solid-liquid phase transitions in CdTe crystals under pulsed laser irradiation," *Applied Physics Letters,* vol. 83, no. 18, pp. 3704-3706, 2003.

[58] V. K. Savchuk, B. K. Kotlyarchuk, A. O. Zaginey, M. Oszwaldowski and J. Rzeszutek, "Ablation Species Generated by High Power Laser Pulses from CdTe Target," in *SPIE: The International Society for Optical Engineering,* USA, 1999.

[59] I. Pelant and J. Valenta, "Luminescence of Excitons," in *Luminescence Spectroscopy of Semiconductors,* Oxford, Oxford University Press, 2012, pp. 161-202.

[60] G. Agostini and C. Lamberti, Characterization of Semiconductor Heterostructures and Nanostructures, Amsterdam: Elsevier, 2008.

[61] G. D. Gilliland, "Photoluminescence Spectroscopy of Crystalline Semiconductors," *Materials Science and Engineering: Reports,* vol. 18, no. 3-6, pp. 99-399, 1997.

[62] L. L. Kazmerski, Polycrystalline and Amorphous Thin Films and Devices (Materials Science and Technology Series), St. Ann Arbor: Academic Press, 1980.

[63] H. Zimmermann, R. Boyn and K. Piel, "Thermal Quenching of Bound Exciton Emission due to Phonon-induced Non-radiative Transitions: Experimental Data for CdTe and InP," *Journal of Physics,* vol. 4, no. 3, 1992.

[64] F. H. Pollak, "Modulation Spectroscopy of Semiconductors: Bulk/thin film, Microstructures, Surfaces/interfaces and Devices," *Materials Science and Engineering: Reports,* vol. 10, no. 7-8, pp. 275-374, 1993.

[65] O. J. Glembocki, B. V. Shanabrook, N. Bottka, W. T. Beard and J. Comas, "Photoreflectance Characterization of Interband Transitions in GaAs/AlGaAs Multiple Quantum Wells and Modulation-doped Heterojunctions," *Applied Physics Letters,* vol. 46, no. 10, pp. 970-972, 1985.

[66] D. G. Seiler and C. L. Littler, "Volume 36," in *Semiconductor and Semimetals,* Elsevier Limited, 1992.

[67] D. E. Aspnes, "Third-derivative Modulation Spectroscopy with Low-field Electroreflectance," *Surface Science,* vol. 37, pp. 418-442, 1973.

[68] H. Shen, Z. Hang, S. H. Pan, F. H. Pollak and J. M. Woodall, "Dependence of the Photoreflectance of Semi-insulating GaAs on Temperature and Pump Chopping Frequency," *Applied Physics Letters,* vol. 52, no. 24, pp. 2058-2060, 1988.

[69] Y. Zhonghai, S. G. Hofer, N. C. Giles, T. H. Myers and C. J. Summers, "Interpretation of Near-band-edge Photoreflectance Spectra from CdTe," *Physical Review B,* vol. 51, no. 19, pp. 13789-13792, 1995.

[70] H. Shen and M. Dutta, "Franz-Keldysh Oscillations in Modulation Spectroscopy," *Journal of Applied Physics,* vol. 78, no. 4, pp. 2151-2177, 1995.

[71] N. D. Bassim, P. K. Schenck, M. Otani and H. Oguchi, "Model, Prediction, and Experimental Verification of Composition and Thickness in Continuous Spread Thin Film combinatorial Libraries Grown by Pulsed Laser Deposition," *Review of Scientific Instruments,* vol. 78, no. 7, pp. 72203-72208, 2007.

[72] Y. Yan, R. G. Dhere, K. M. Jones and M. M. Al-Jassim, "Influence of Substrate Structure on the Growth of CdTe Thin Films," *Journal of Applied Physics,* vol. 89, no. 11, pp. 5844-5848, 2001.

[73] Y. Yan, M. M. Al-Jassim and T. Demuth, "Energetics and Effects on Planar Defects in CdTe," *Journal of Applied Physics,* vol. 90, no. 8, pp. 3952-3955, 2001.

[74] École Polytechnique de Montréal, "SGTE Binary Alloy Database," Centre for Research in Computational Thermochemistry, November 2011. [Online]. Available: http://www.crct.polymtl.ca/fact/documentation/BINARY/BINARY_list.htm.

[75] A. S. Jordan and R. R. Zupp, "Calculation of the p-T Diagrams of CdTe," *Journal of the Electrochemical Society,* vol. 116, no. 9, pp. 1285-1286, 1969.

[76] J. J. Dubowski, J. M. Wrobel and D. F. Williams, "Dependance of the Vacuum Sublimation Rate of CdTe upon Crystallographic Orientation," *Applied Physics Letters,* vol. 53, no. 8, pp. 660-662, 1988.

[77] P. W. Sze, K. F. Yarn, Y. H. Wang, M. P. Houng and G. L. Chen, "Characteristics of MOCVD-Grown," *Active and Passive Electronic Components,* vol. 18, no. 4, pp. 247-258, 1995.

[78] Q. Jiang, J. T. Mullins, J. Toman, Hase, P. A. Thomas, B. J. Cantwell, G. Lloyd, A. Basu and A. W. Brinkman, "Hetero-epitaxial Crystal Growth of CdTe on GaAs Substrates," *Journal of Crystal Growth,* vol. 310, no. 7-9, pp. 1652-1656, 2008.

[79] Z. H. Wu, T. Tanikawa, T. Murase, Y. Y. Fang, C. Q. Chen, Y. Honda, M. Yamaguchi, H. Amano and N. Sawaki, "Partial Strain Relaxation by Stacking Fault Generation in InGaN Multiple Quantum Wells Grown on (101) Semipolar GaN," *Applied Physics Letters,* vol. 98, no. 5, pp. 51902-51904, 2011.

[80] R. K. Willardson and A. C. Beer, "Volume 8: Transport and Optical Phenomena," in *Semiconductors and Semimetals,* New York, Academic Press, 1972.

[81] H. Shen, S. H. Pan and F. H. Pollak, "Conclusive Evidence for Miniband Dispersion in the Photoreflectance of a GaAs/Ga0.74Al0.26As Coupled Multiple-quantum-well Structure," *Physical Review B,* vol. 36, no. 17, pp. 9384-9387, 1987.

[82] A. N. Pikhtin and A. D. Yas'kov, "Refraction of Light in Semiconductors (Review)," *Soviet Physics: Semiconductors,* vol. 22, no. 5, pp. 613-626, 1988.

[83] F. Dal'Bo, G. Lentz, N. Magnea, H. Mariette, L. S. Dang and J. L. Pautrat, "Spectroscopic Study of CdTe Layers Grown by Molecular-beam Epitaxy on (001) and (111) Cd0.96Zn0.04Te Substrates," *Journal of Applied Physics,* vol. 66, no. 3, pp. 1338-1346, 1989.

[84] C. E. Barnes and K. Zanio, "Photoluminescence in High-resistivity CdTe : In," *Journal of Applied Physics,* vol. 46, no. 9, pp. 3959-3964, 1975.

[85] O. Osamu, Compound Semiconductor Bulk Materials and Characterizations, New Jersey: World Scientific Pub. Co. Inc., 2007.

[86] S. Hildebrandt, H. Uniewski, J. Schreiber and H. S. Leipner, "Localization of Y Luminescence at Glide Dislocations in Cadmium Telluride," *Journal De Physique III,* vol. 7, no. 7, pp. 1505-1514, 1997.

[87] S. T. Edwards, A. F. Schreiner, T. M. Myers and J. F. Schetzina, "Photoluminescence from CdTe/sapphire Films Prepared by Molecular Beam Epitaxy," *Journal of Applied Physics,* vol. 54, no. 11, pp. 6785-6786, 1983.

[88] Y. P. Varshni, "Temperature Dependence of the Energy Gap in Semiconductors," *Physica,* vol. 34, no. 1, pp. 149-154, 1967.

[89] A. Manoogian and J. C. Woolley, "Temperature Dependence of the Energy Gap in Semiconductors," *Canadian Journal of Physics,* vol. 62, no. 3, pp. 285-287, 1984.

[90] S. S. Choi and G. Lucovsky, "Native Oxide Formation on CdTe," *Journal of Vacuum Science & Technology B,* vol. 6, no. 4, pp. 1198-1203, 1988.

[91] Z. Yu, S. G. Hofer, N. C. Giles, T. H. Myers and C. J. Summers, "Interpretation of Near-band-edge Photoreflectance Spectra from CdTe," *Physical Review B,* vol. 51, no. 19, pp. 13789-13792, 1995.

[92] J. Lee, N. C. Giles, D. Rajvel and C. J. Summers, "Room-temperature Band-edge Photoluminescence from CdTe Telluride," *Physical Review B,* vol. 49, no. 3, pp. 1668-1676, 1994.

[93] F. G. Sánchez-Almazan, H. Navarro-Contreras, G. Ramírez-Flores, M. A. Vidal, O. Zelaya-Angel, M. E. Rodríguez and R. Baquero, "Temperature Dependence of the Band Gap of Cd1-xZnxTe Alloys of Low Zinc Concentrations," *Journal of Applied Physics,* vol. 79, no. 10, pp. 7713-7717, 1996.

[94] R. M. Cannon, R. M. Fisher and A. G. Evans, "Decohesion of Thin Films from Ceramic Substrates," in

MRS Proceedings: Thin Films - Interfaces and Phenomena, 1985.

[95] H. H. Yu, M. Y. He and J. W. Hutchinson, "Edge Effects in Thin Film Delamination," *Acta Materialia,* vol. 49, no. 1, pp. 93-107, 2001.

[96] H. H. Yu and J. W. Hutchinson, "Delamination of Thin Film Strips," *Thin Solid Films,* vol. 423, no. 1, pp. 54-63, 2003.

[97] V. Lyahovitskaya, L. Chernyak, J. Greenberg, L. Kaplan and D. Cahen, "Low Temperature, Postgrowth Self-doping of CdTe Single Crystals due to Controlled Deviation from Stoichiometry," *Journal of Applied Physics,* vol. 88, no. 7, p. 3981, 2000.

[98] T. H. Myers, N. C. Giles-Taylor, R. W. Yanka, R. N. Bicknell, J. W. Cook, J. F. Schetzina, S. R. Jost, H. S. Cole and H. H. Woodbury, "Properties and Applications of CdTe/Sapphire Epilayers Grown by Molecular Beam Epitaxy," *Journal of Vacuum Science & Technology A,* vol. 3, no. 1, pp. 71-74, 1985.

Appendices

Appendix A- Defect Formation Energy for Common Extrinsic and Intrinsic Dopants in CdTe

Defect	Formation Energy (eV)	Defect	Formation Energy (eV)
V_{Cd}	2.67	Cu_{Cd}	1.31
V_{Te}	3.24	Ga_{Cd}	1.23
Cd_{Te}	3.92	As_{Te}	1.68
Te_{Cd}	3.70	Ag_{Cd}	1.32
T_i	3.41	In_{Cd}	1.23
Cd_i^a	2.26	Sb_{Te}	1.72
Cd_i^c	2.04	Au_{Cd}	1.30
O_{Cd}	-0.41	Bi_{Te}	1.96
F_{Te}	-0.08	Na_i^a	0.60
Na_{Cd}	0.45	Na_i^c	0.45
Al_{Cd}	1.17	Cu_i^a	2.14
P_{Te}	1.83	Cu_i^c	2.24
Cl_{Te}	1.23		

Table 1: Calculated Formation and Defect Transition Energy Levels of Point Defects from a Neutral Charge State, Modified from [20]

Appendix B- Substrate Degreasing Standard Operating Procedure

Preface

The necessity to clean a substrate before attempting epitaxial growth is not a function of the cleanliness of the product manufactured but from contamination that might occur after opening and cleaving the original substrate into smaller pieces. Substrates purchased are often manufactured and prepared in rooms with a much higher level of cleanliness, rated by the number of particles of a given size in units of microns which occupy a given cubic meter of space in the workspace, than the laboratory. As such, the grower presents the biggest source of contamination to the substrate, followed by the cleanliness of the laboratory workspace, laboratory equipment and utensils, and laboratory airspace.

When handling substrates in the lab always ensure protective gloves and goggles are worn to avoid contamination of the substrate or self-exposure to the chemicals being used. Holding and working with the substrates away from one's person is an easy way to lessen the effect of contamination that person will have on the substrate. Furthermore, restrain opening the mouth or excess movement as they can provide further sources of contaminants. Use clean tweezers instead of gloves whenever possible to move and handle substrates.

The lab workspace may be shared with an office where food and drink are sometimes consumed. Do not attempt to clean a substrate if food, particularly oily food, is noticed by smell in the office space because it is likely to have travelled into the laboratory space. Oils and polymers are exceptionally difficult to remove from surfaces. The same can be

said about fine particulates because of stiction. Ensure that cleaved samples are frequently dusted and cleaved in such a way that prevents the settling of material onto the substrate.

Maintaining the cleanliness of the substrate should not end after its solvent sonication or after a film has been deposited on it. The careful handling of substrates and samples will ensure better quality photo-masks, contacts and devices. Essentially, maintaining sample cleanliness in all processes will improve the reproducibility of samples and measurement precision.

Experimental Setup

Before to beginning the sonication cleaning procedure, please ensure the following is complete in listed order:

1. Ensure the availability of safety equipment, acrylic or latex gloves and chemically protective eyewear and then use as directed.
2. From the flammables cabinet remove the acetone, methanol, isopropanol and waste container. Top up the spray bottles as necessary and place a glass solvent waste funnel in the waste container.
3. Using paper towels and methanol clean a workspace on the countertop.
4. Ensure that the water in the sonication chamber is clean and filled to the appropriate level. If the water is dirty, change the water using a beaker a ‘scoop’ and pour out the dirty water into the sink. Fill the sonication chamber with clean cold tap water to a depth of approximately 1 inch.

5. Lay out clean lens paper to place utensils and substrates on during the cleaning procedure. Never place anything on the countertop directly except for the beaker which holds the substrates, substrate holder and tweezers. This is to prevent contamination of the outside of the beaker onto lens paper. The beaker can be placed on a piece of laid out paper towel if necessary.

Experimental Procedure

It is assumed that this procedure will occur after substrates have been cleaved to the appropriate dimensions, 12mm by 12mm squares. However, it can be carried out on substrates of any geometry or size within the limitations of the substrate holder size and handling. Be sure to change gloves frequently and that those gloves are appropriate for the solvents involved in this process.

1. Rinse the inside of the beaker, the tweezers and the substrate holder over the waste solvents funnel with isopropanol, methanol and acetone in that order for ten seconds each with each solvent. When rinsing the inside of the beaker, avoid cross contamination of the inside of the beaker from solvents and materials on the outside of the beaker. This is best accomplished on a beaker with water contamination on the outside wall by rinsing the outside of the beaker with solvents prior cleaning the inside.
2. Rinse the inside of the beaker, the tweezers and the substrate holder over the waste solvents funnel with acetone, methanol and isopropanol in that order ten seconds each with each solvent.

3. Holding the substrate with tweezers, rinse off the substrate with isopropanol, methanol and acetone in that order and then acetone, methanol and isopropanol in that order. Each solvent rinse should last ten seconds, approximately 5 seconds per side of the substrate.
4. While holding the substrate with tweezers use a foam tip applicator soaked in isopropanol to wipe one side of the substrate from left to right across the entire substrate. Approximately every 20 seconds rotate the substrate 90 degrees while wiping the same face. This ensures that particles on all sides of the substrate side are wiped away. Continue to wipe the first side of the substrate for 1 minute. If you have to put the substrate down for whatever reason do so on lens paper.
5. Repeat step 4 on the second side of substrate using a new foam tip applicator and place the substrate upright in the substrate holder. The substrate holder should be resting on a clean piece of lens paper.
6. Change gloves and repeat steps 3, 4 and 5 as necessary for all substrates. Holding the filled substrate holder above the waste solvent funnel rinse the substrates in isopropanol, methanol and acetone in that order for ten seconds each with each solvent. Then rinse the filled substrate holder above the waste solvent funnel in isopropanol for 30 seconds.
7. Place the filled substrate holder inside the cleaned beaker and fill with isopropanol. The level of solvent in the beaker should be approximately 0.5cm higher than the top of the tallest substrate in the holder. Place the tweezers into the filled beaker onto the substrate holder in a position that will ensure no contact between the tweezers and the substrates during sonication.

8. Place the filled beaker into the sonicator. The water level in the sonicator should be equivalent to the solvent level in the beaker. Turn on the sonicator and set the time to 45 minutes. Start the sonication cycle and wait.
9. When sonication in isopropanol is complete take filled substrate holder and tweezers out of beaker and place on lens paper. Rinse the inside of the beaker over the waste solvent funnel with isopropanol, and then methanol for 10 seconds each. Make sure to not cross contaminate the substances on the outside of the beaker with the inside of the beaker. This is best accomplished by first solvent rinsing the outside of the beaker of water and contaminants.
10. Place beaker onto previously laid out paper towel and then rinse filled substrate holder over waste solvent funnel with isopropanol and then methanol for 10 seconds each.
11. Repeat steps 7 and 8 replacing the use of isopropanol for methanol.
12. When sonication in methanol is complete take filled substrate holder and tweezers out of beaker and place on lens paper. Rinse the inside of the beaker over the waste solvent funnel with methanol, and then acetone for 10 seconds each. Make sure to not cross contaminate the substances on the outside of the beaker with the inside of the beaker. This is best accomplished by first solvent rinsing the outside of the beaker of water and contaminants.
13. Place beaker onto previously laid out paper towel and then rinse filled substrate holder over waste solvent funnel with methanol and then acetone for 10 seconds each.
14. Repeat steps 7 and 8 replacing the use of methanol for acetone. The sonication time should also be extended to 75 minutes instead of 45 minutes. Set a timer to 40 minutes to

run concurrently with the sonicator. Check the progress of this sonication at 40 minutes into the cycle and top up the acetone in the beaker as necessary. Of all the solvents it is the most likely to evaporate away during sonication. Do not let the beaker evaporate dry. In the case that the solvent level drops below the substrates, top up the acetone level to above the substrates and extend the sonication by 10 minutes.

15. While the acetone sonication is in progress it, prepare the substrate case where the samples will be kept by rinsing in methanol over the waste funnel as necessary and then drying with dry $N_{2(g)}$.
16. When sonication in acetone is complete take filled substrate holder and tweezers out of beaker and place on lens paper. Rinse the inside of the beaker over the waste solvent funnel with acetone for 10 seconds. Make sure to not cross contaminate the substances on the outside of the beaker with the inside of the beaker. This is best accomplished by first solvent rinsing the outside of the beaker of water and contaminants.
17. Place beaker onto previously laid out paper towel and then rinse filled substrate holder over waste solvent funnel with acetone and then methanol for 10 seconds each.
18. Using the tweezers, gently clamp the side of a substrate and remove it from the substrate holder. Rinse both sides of the substrate with methanol for 15 seconds. Still holding the substrate in the tweezers, use dry $N_{2(g)}$ to dry both sides of the substrate gently. Ensure restricted flow of the dry $N_{2(g)}$ to prevent the substrate from slipping from the tweezers.

Note If the acetone is heated slightly to 30° C for the last sonication process it will not be necessary to rinse substrates finally in acetone and methanol as well as dry samples with $N_{2(g)}$. Substituting a heated acetone sonication, the solvent should evaporate quickly

enough from samples removed from the beaker that they can be stored directly. Caution is advised since excess acetone will affect storage containers adversely, however, heated acetone sonication has been shown to be a superior technique to the acetone and methanol end step rinse via optical microscopy of cleaned samples.

19. Store the substrate in the cleaned substrate case, growth side up, and replace the substrate case lid.
20. Repeat steps 18 and 19 for any remaining substrates.
21. Clean off any remaining utensils as necessary with methanol, and then return the substrate holder and tweezers to the beaker. Cut a piece of wax paper slightly bigger than the projected top area of the cylinder. Cover the beaker containing the substrate holder and tweezers with wax paper and store on shelf for later use.
22. Return all solvents spray bottles and waste solvents to the flammables cabinet. Return the waste solvent funnel to its holder above the sink.
23. Store filled substrate case away from potential sources of contaminants, such as condensing water, on a flat surface.

Appendix C- Raw and Unfiltered PL Spectrum

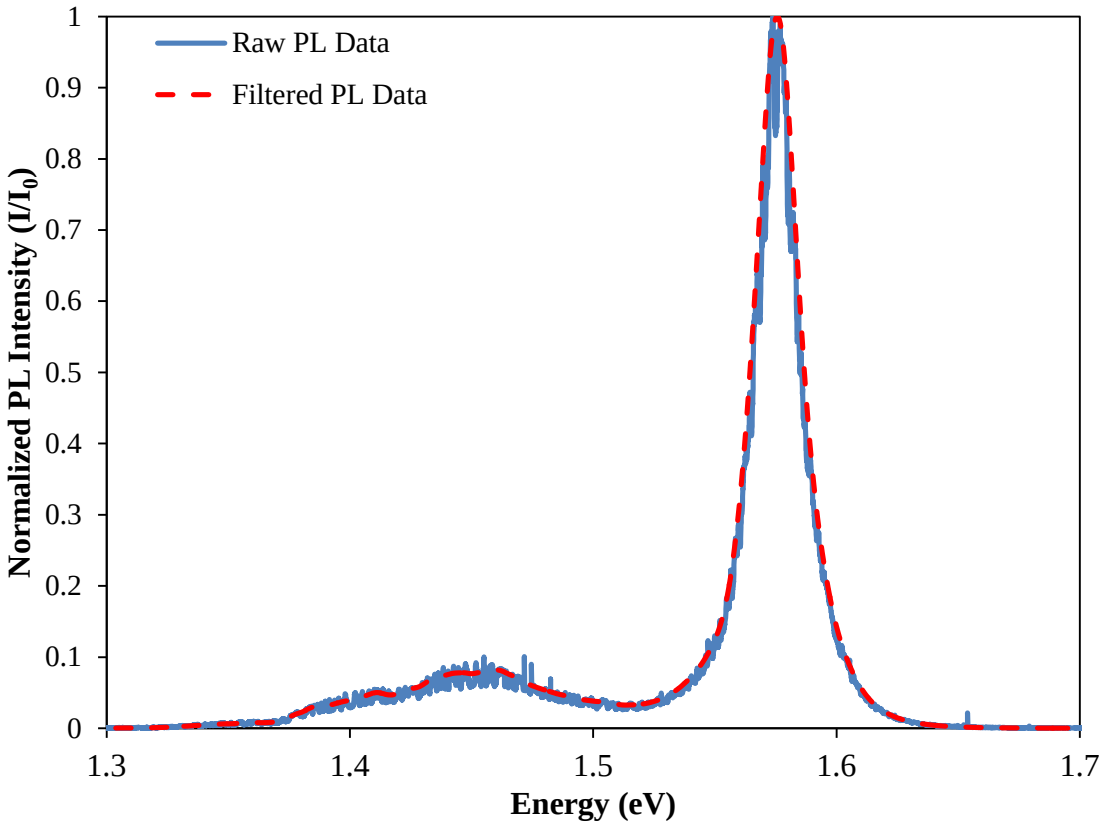

Figure 31: Raw Unfiltered PL Spectrum Superimposed on Low Pass and Median Filtered Spectrum